Available online at www.sciencedirect.com
SCIENCE DIRECT®
Comput. Methods Appl. Mech. Engrg. 193 (2004) 1171–1202
Computer methods in applied mechanics and engineering
www.elsevier.com/locate/cma

# Positivity conditions in meshless collocation methods

Xiaozhong Jin, Gang Li, N.R. Aluru *

*Department of Mechanical and Industrial Engineering, Beckman Institute for Advanced Science and Technology, University of Illinois at Urbana-Champaign, Urbana, IL 61801, USA*

Received 19 March 2003; received in revised form 3 October 2003; accepted 4 December 2003

**Abstract**

Collocation meshless methods are conceptually simple, easy-to-implement and fast numerical methods. The robustness of collocation methods has, however, been an issue especially for scattered set of points. In this paper we show that the robustness of collocation meshless methods can be improved by ensuring that certain conditions, defined as the positivity conditions, are satisfied when constructing approximation functions and their derivatives. The significance of positivity conditions is pointed out by an error analysis of the finite cloud method, which is a collocation based meshless method. We propose techniques, based on modification of weighting functions, to ensure satisfaction of positivity conditions on the approximation function and its derivatives when using a scattered set of points. Several types of weighting functions are tested for 1D and 2D problems on scattered points. Numerical results demonstrate the effectiveness of collocation methods when positivity conditions are satisfied.


*Keywords:* Positivity conditions; Collocation methods; Finite cloud method; Error analysis; Weighting function

## 1. Introduction

Meshless methods have emerged as a class of effective numerical methods which are capable of avoiding the difficulties encountered in conventional computational mesh based methods, such as, meshing complex geometries, mesh distortion due to large deformation and remeshing in moving boundary problems. Extensive research has been conducted in the area of meshless methods in recent years (see [1] for an overview). Broadly defined, meshless methods contain two key steps: construction of meshless approximation functions and their derivatives and meshless discretization of the governing partial–differential equations. Least-squares and kernel based approaches are two techniques that have gained considerable attention for construction of meshless approximation functions (see [2] for a detailed discussion on least-squares and kernel approximations). The meshless discretization of the partial–differential equations can be

* Corresponding author.
*E-mail address:* aluru@uiuc.edu (N.R. Aluru).
*URL:* http://www.staff.uiuc.edu/~aluru.

0045-7825/$ - see front matter © 2004 Published by Elsevier B.V.
doi:10.1016/j.cma.2003.12.013

categorized into three classes: cell integration [3–5], local point integration [6], and point collocation [7–11]. Of these techniques, point collocation is the simplest approach. Oñate et al. [7,8], Liszka et al. [9], Aluru [10] and Aluru and Li [11] have reported satisfactory results for a large class of problems encountered in engineering applications. However, the robustness of the collocation approach is an issue especially when scattered and random points are used to discretize the governing equations. For example, Oñate et al. [7,8] have noticed some stability problems when applying the point collocation method to fluid flow problems. Benito et al. [12] have reported that the solution of the generalized finite-difference method depends on the number of nodes in the cloud, the relative position of the nodes in the cloud with respect to the star node and the weighting function.

In this paper, we try to improve the robustness of the collocation methods by understanding the possible sources of error that arise when using a scattered point of points. Specifically, the errors could arise because of the way the meshless approximation functions and their derivatives have been constructed for a scattered point of points or because of the way the discretization of the governing equations has been performed. Instead of using a straight-forward point collocation technique for discretization, it is possible to use more sophisticated collocation methods which could minimize solution errors for a scattered set of points. We leave this topic for future research and in this paper we address the issue of improving the quality of the approximation functions and its derivatives when using a scattered set of points. We observed that when the meshless approximation functions and its derivatives do not satisfy certain conditions (referred to as the positivity conditions) for a given point distribution, it is possible to get large numerical errors when using collocation methods. To satisfy the positivity conditions, the weighting function used in the construction of the approximation functions can play an important role. The positivity conditions are well-known in the literature for over five decades now [13]. Patankar [14] included the positivity conditions in a series of basic rules for constructing finite-difference schemes. Demkowicz et al. [15] proved that ensuring positivity conditions is sufficient to prove convergence of the finite-difference method on arbitrary irregular meshes for some class of elliptic problems. Liszka et al. [9] used the positivity conditions to explain the better solutions obtained from the Hermite-type approximations. These studies suggest that positivity conditions can be important when using meshless collocation methods.

The objective of this paper is to develop appproaches to satisfy positivity conditions in the finite cloud method [2,10,11], which employs a fixed kernel technique for the construction of interpolation functions and a point collocation technique for the discretization of the governing equations. We perform an error analysis of the finite cloud method to investigate the importance of the positivity conditions. We then propose techniques to enforce the satisfaction of the positivity conditions by customizing weight functions. The rest of the paper is outlined as follows: Section 2 summarizes the finite cloud method, Section 3 summarizes the positivity conditions and their significance by considering a numerical example, Section 4 presents an error analysis of the finite cloud method, Sections 5 and 6 describe approaches to satisfy the positivity conditions in 1D and 2D domains, respectively, and numerical examples with scattered point distributions are given in Section 7. Finally, conclusions are given in Section 8.

## 2. Finite cloud method

The finite cloud method (FCM) employs a fixed kernel technique to construct the meshless approximation functions and a point collocation technique to discretize the governing partial differential equations. In the following, we outline the steps used for the construction of approximation functions (see [2,11] for more details). Let the domain $\Omega \in \mathbb{R}^d$ ($d$ is the dimension) denote an open bounded connected set of points in $\mathbb{R}^d$. A point in $\mathbb{R}^d$ is denoted by $\mathbf{x} = \{x_1, \ldots, x_d\}$. The domain $\Omega$ is first represented by a set of $NP$ points (or nodes), as shown in Fig. 1 for two-dimensions. Then, for each node an approximation function is generated by constructing a cloud about that node (also referred to as a star node). A cloud is constructed

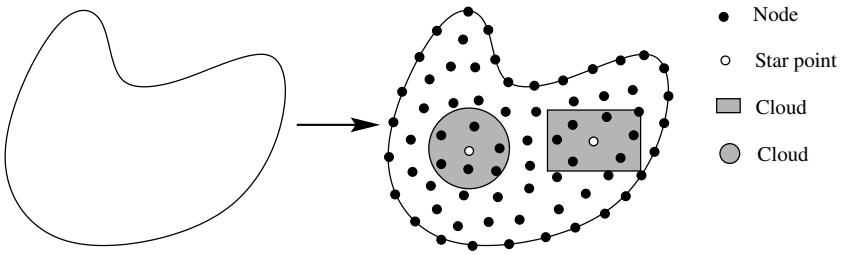


Fig. 1. Physical domain (left) is represented by a set of points (right). Clouds are constructed at each point. Also shown in the figure are circular and rectangular clouds.

by centering a kernel about the star point. The kernel is non-zero at the star point and at few other nodes that are in the vicinity of the star point. The shape of the cloud, which defines the nodes at which the kernel is non-zero, can be arbitrary. Typical shapes we have employed are circles and rectangles in 2D. In a fixed kernel approach, an approximation $u^a(\mathbf{x})$ to an unknown $u(\mathbf{x})$ is given by

$$u^a(\mathbf{x}) = \int_\Omega \mathscr{C}(\mathbf{x}, \mathbf{x}_k - \mathbf{y})\phi(\mathbf{x}_k - \mathbf{y})u(\mathbf{y})\,\mathrm{d}\mathbf{y}, \tag{1}$$

where $\phi$ is the kernel function centered at $\mathbf{x}_k$ and $\mathscr{C}(\mathbf{x}, \mathbf{x}_k - \mathbf{y})$ is the correction function which is given by

$$\mathscr{C}(\mathbf{x}, \mathbf{x}_k - \mathbf{y}) = \mathbf{p}^{\mathrm{T}}(\mathbf{x}_k - \mathbf{y})\mathbf{c}(\mathbf{x}), \tag{2}$$

where $\mathbf{p}(\mathbf{x}_k - \mathbf{y})$ is an $m \times 1$ vector of shifted polynomial basis and $\mathbf{c}(\mathbf{x})$ is the unknown correction function vector (see [2,11] for details) and $(x_k, y_k)$ is the center of the kernel function. In constructing the approximation function for a point $(x, y)$, one can choose $(x_k, y_k)$ arbitrarily and consequently the approximation function can be multivalued. A unique set of interpolation functions can be constructed by fixing $(x_k, y_k)$ at the point $(x, y)$, i.e., when computing $N_i(x, y)$, $i = 1, 2, \ldots, NP$ and its derivatives, the center of the kernel function is fixed at $(x, y)$ (see [11] for more details). In discrete form, the approximation in Eq. (1) can be written as

$$u^a(\mathbf{x}) = \sum_{i=1}^{NP} N_i(\mathbf{x})\hat{u}_i, \tag{3}$$

where $\hat{u}_i$ is the nodal parameter for node $i$, and $N_i(\mathbf{x})$ is the fixed kernel meshless approximation function defined as

$$N_i(\mathbf{x}) = \mathbf{p}^{\mathrm{T}}(\mathbf{x})\mathbf{M}^{-\mathrm{T}}\mathbf{p}(\mathbf{x}_k - \mathbf{x}_i)\phi(\mathbf{x}_k - \mathbf{x}_i)\Delta V_i, \tag{4}$$

where $\Delta V_i$ is the nodal volume and $\mathbf{M}$ is the moment matrix. The $ij$th entry in the moment matrix is given by

$$M_{ij} = \sum_{l=1}^{NP} p_i(\mathbf{x}_k - \mathbf{x}_l)\phi(\mathbf{x}_k - \mathbf{x}_l)p_j(\mathbf{x}_l)\Delta V_l \quad i, j = 1, 2, \ldots, m. \tag{5}$$

Let the $\alpha$th order partial derivative of a function $u$ be denoted by

$$D^\alpha u(\mathbf{x}) = \frac{\partial^{|\alpha|} u(\mathbf{x})}{\partial^{\alpha_1} x_1, \ldots, \partial^{\alpha_d} x_d} \quad |\alpha| = \sum_{i=1}^{d} \alpha_i. \tag{6}$$

The derivatives of the unknown $u$ are approximated by

$$D^{\alpha}u^{a}(\mathbf{x}) = \sum_{i=1}^{NP} D^{\alpha}N_i(\mathbf{x})\hat{u}_i. \tag{7}$$

After the meshless approximation functions are constructed, the FCM uses a point collocation technique to discretize the governing equations. For nodes with prescribed boundary conditions the approximate solution or the derivative of the approximate solution are set to the given Dirichlet and Neumann-type boundary conditions, respectively. The point collocation approach gives rise to a linear system of equations, the solution of which provides the nodal parameters at the nodes. Once the nodal parameters are computed, the unknown solution at each node can be computed from Eq. (3).

## 3. Positivity conditions

The positivity conditions [13], as commonly referred to in the finite difference literature, on the approximation function and its second-order derivatives are stated as

$$N_i(\mathbf{x}_j) \geqslant 0, \tag{8}$$

$$\nabla^2 N_i(\mathbf{x}_j) \geqslant 0 \quad j \neq i, \tag{9}$$

$$\nabla^2 N_i(\mathbf{x}_i) < 0, \tag{10}$$

where $N_i(\mathbf{x}_j)$ is the approximation function of a point $i$ evaluated at a point $j$. In the 2D case, Eqs. (9) and (10) can be written as

$$\frac{\partial^2 N_i(x_j, y_j)}{\partial x^2} + \frac{\partial^2 N_i(x_j, y_j)}{\partial y^2} \geqslant 0 \quad j \neq i, \tag{11}$$

$$\frac{\partial^2 N_i(x_i, y_i)}{\partial x^2} + \frac{\partial^2 N_i(x_i, y_i)}{\partial y^2} < 0. \tag{12}$$

It has been shown that the satisfaction of Eqs. (8)–(10) ensures the convergence of the finite-difference method with arbitrary irregular meshes for some class of elliptic problems [15]. Patankar [14] included the positivity conditions in a series of basic rules for the construction of finite differences and pointed out that the consequence of violating the positivity conditions gives a physically unrealistic solution. To understand the significance of positivity conditions in meshless collocation methods, we consider a one-dimensional Poisson equation of the form

$$\frac{\partial^2 u}{\partial x^2} = -6x - \left(\frac{2}{\alpha^2} - 4\frac{(x-\beta)^2}{\alpha^4}\right)\exp\left[-\frac{(x-\beta)^2}{\alpha^2}\right] \quad 0 \leqslant x \leqslant 1. \tag{13}$$

A Dirichlet boundary condition is applied at $x = 0$ and a Neumann boundary condition is applied at $x = 1$. $\alpha$ and $\beta$ are chosen to be 0.2 and 0.5, respectively. The exact solution of this problem is

$$u = -x^3 + \exp\left[-\frac{(x-\beta)^2}{\alpha^2}\right]. \tag{14}$$

The finite cloud method is used to solve this problem. In the implementation of FCM, a Gaussian weighting function and 21 uniformly distributed points are employed. The Gaussian weighting function is given by

$$\phi(x_i - x) = \frac{e^{-\left(\frac{x_i - x}{c}\right)^2} - e^{-\left(\frac{d_{m_i}}{c}\right)^2}}{1 - e^{-\left(\frac{d_{m_i}}{c}\right)^2}}, \tag{15}$$

where $d_{m_i}$ is the cloud (support) size and $c$ is the dilation parameter ($c$ is chosen as $d_{m_i}/2$) that defines the steepness of the curve.

The error in the numerical solution is measured by

$$\varepsilon = \frac{1}{|u|_{\max}} \sqrt{\frac{1}{NP} \sum_{i=1}^{NP} [u(\mathbf{x}_i) - u^a(\mathbf{x}_i)]^2}, \tag{16}$$

where $\varepsilon$ is the error, $u$ and $u^a$ denote, respectively, the exact and the computed solutions.

It can be shown that, when 3 point clouds are used, the 1D fixed kernel approximation functions with the quadratic basis are identical to the second-order finite-difference stencils. Therefore, the positivity conditions (Eqs. (8)–(10)) are all satisfied. However, when the cloud size is increased, the positivity conditions are violated. Fig. 2 shows the approximation function centered at $x = 0.5$ and its second-derivative when the cloud size is 3 points, 5 points, 7 points and 11 points. As shown in Fig. 2, when a 5 point cloud is used, the second and third positivity conditions (Eqs. (9) and (10), respectively) are still satisfied, i.e., the second derivative of the approximation function is negative for the star node and positive for all the other points in the cloud. However, the first positivity condition is violated since the approximation function becomes negative for certain points. When the cloud size is enlarged to cover 7 points, the two nodes near the star point start to have negative values for the second derivative of the approximation function. Hence, the second positivity condition is also violated. Moreover, the ratio of the negative values at the nearby points to the value at the star point increases as the cloud size increases. Fig. 3 is a plot of the global error (computed by using Eq. (16)) as a function of the cloud size. As shown in Fig. 3, the global error is small for 3 point clouds and increases as the cloud size increases. When the positivity conditions are violated (starts from a cloud size of 5 points), the error increases dramatically.

For a scattered point distribution, the positivity conditions are more likely to be violated. Therefore, meshless collocation methods can be sensitive to the location of the points and the cloud size, especially when there are less number of points and the point distribution is highly irregular.

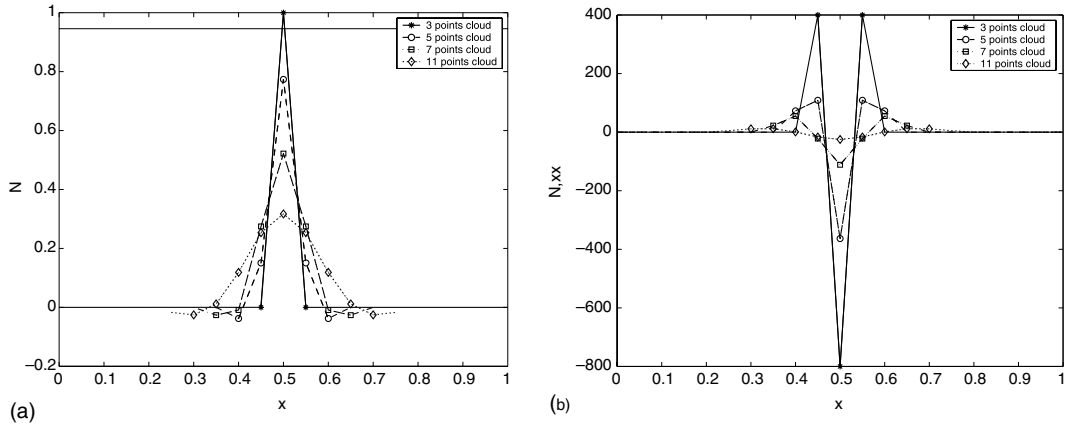


Fig. 2. Shape function (a) and the second derivative of the shape function (b) for various cloud sizes.

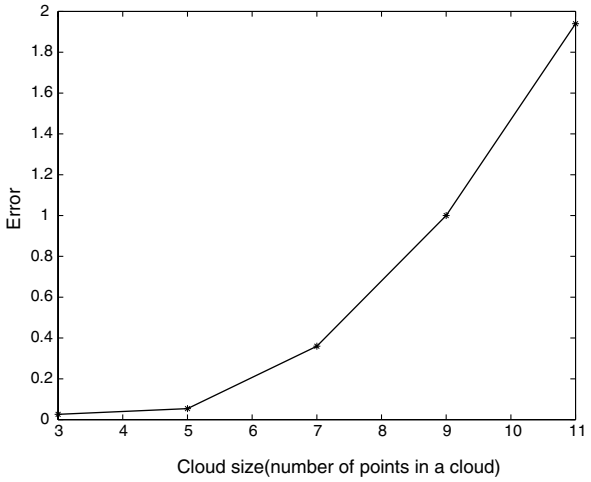


Fig. 3. Error in the numerical solution as a function of cloud size.

## 4. Error analysis of the finite cloud method

In FCM, the numerical error comes from two sources: approximation error and discretization error. In this section, we derive mathematical expressions for the error bound of the FCM solution. It is shown that the global error is proportional to the cloud size and the condition number of the final coefficient matrix which is closely related to the positivity conditions.

### 4.1. Definitions and notation

The Lebesgue space $L^p(\Omega)$ [16] are classes of functions $u(\mathbf{x})$ that are Lebesgue-measurable on $\Omega$ and for which $|u(\mathbf{x})|^p$ is Lebesgue-summable, i.e.,

$$L^p(\Omega) = \left\{ u \middle| \int |u(\mathbf{x})|^p \, d\mathbf{x} < \infty \right\}, \quad 1 \leqslant p \leqslant \infty. \tag{17}$$

Sobolev spaces [16] are classes of Lebesgue-measurable functions which are defined as

$$W^{m,p}(\Omega) = \{u | u \in L^p(\Omega) : D^\alpha u \in L^p(\Omega) \quad \text{for } |\alpha| \leqslant m\}. \tag{18}$$

The spaces of interest in this paper are for $p = 2$. These spaces are Hilbert spaces denoted by $H^m(\Omega) = W^{m,2}(\Omega)$.

### 4.2. Bounds for approximation functions

The bounds for the moving reproducing kernel approximation functions and its derivatives have been discussed in [17–19]. It is easy to show that the conclusions drawn in [17] are also valid for the fixed kernel approximation. From the results of [17, Theorem 4.7], we can derive the following:

**Theorem 1.** *Assume the weighting function $\phi \in C^0$ and the point distributions are regular, then there is a constant $c < \infty$ such that*

$$\max_{1\leqslant i\leqslant NP}\max_{\beta:|\beta|=l}\|D^{\beta}N_i\|_{\infty}\leqslant\frac{c}{r^l}\quad l\geqslant 0 \tag{19}$$

*in particular, if* $|\beta|=0$,

$$\max_{1\leqslant i\leqslant NP}\|N_i\|_{\infty}\leqslant c, \tag{20}$$

*where* $r>0$ *is a generalized support (or cloud) size such that, for a regular point distribution with support sizes* $r_i$, $i=1,\ldots,NP$, *there exist two constants* $c_1,c_2\in(0,\infty)$ *and*

$$c_1\leqslant\frac{r_i}{r}\leqslant c_2\quad\forall i. \tag{21}$$

The regularity of the point distribution [17] implies that, in a cloud, the points are distributed in such a way that the moment matrix is non-singular. Note that in the fixed kernel approximation, the continuity requirement of the kernel function $\phi$ is relaxed compared to the moving reproducing kernel approximation as no differentiation of $\phi$ is required in the fixed kernel approximation.

### 4.3. Error estimates for fixed kernel approximation

In the fixed kernel technique, the approximation to the unknown $u(\mathbf{x})$ is defined by

$$u^a(\mathbf{x})=\sum_{i=1}^{NP}N_i(\mathbf{x})\hat{u}(\mathbf{x}_i). \tag{22}$$

**Theorem 2.** *Assume the weighting function* $\phi\in C^0(\overline{\Omega})$, *the polynomial basis is complete to the mth order and the point distributions are regular. If* $\hat{u}(\mathbf{x})\in C^{m+1}(\overline{\Omega})\cap H^{m+1}(\Omega)$ *and the point-wise overlap condition* [21] *holds, i.e.,*

$$\exists M\in\mathbb{N}\quad\forall\mathbf{x}\in\Omega\quad card\{j|\mathbf{x}\in\Omega_j\}\leqslant M \tag{23}$$

*then the fixed kernel approximation error estimate is given by*

$$\|u^a(\mathbf{x})-\hat{u}(\mathbf{x})\|_{H^0(\Omega)}\leqslant C\cdot r^{m+1}\|\hat{u}(\mathbf{x})\|_{H^{m+1}(\Omega)}\quad 0<C<\infty. \tag{24}$$

**Proof.** We use some concepts and results about polynomial approximations in Sobolev space shown in [17,20, Chapter 4]. Let $\Omega_j$ be the cloud (or support) for a point $\mathbf{x}$. We can choose a ball $B_j$ in $\Omega_j$ such that $\Omega_j$ is star-shaped with respect to $B_j$ [17]. Given $\hat{u}(\mathbf{x})\in C^{m+1}(\overline{\Omega})\cap H^{m+1}(\Omega)$, $Q^{m+1}\hat{u}$ is the Taylor polynomial of order $m$ of $\hat{u}$ averaged over a ball $B_j\subset\subset\Omega$. $Q^{m+1}\hat{u}$ is defined as [20, Chapter 4]

$$Q^{m+1}\hat{u}(\mathbf{x})=\int_{B_j}\sum_{|\alpha|\leqslant m}\frac{(\mathbf{x}-\mathbf{y})^{\alpha}}{\alpha!}D^{\alpha}\hat{u}(\mathbf{y})\phi(\mathbf{y})\,\mathrm{d}\mathbf{y}, \tag{25}$$

where $\phi(\mathbf{y})$ is the cut-off function supported in $\bar{B}_j$. The $m+1$th order residual term is given by

$$R^{m+1}\hat{u}(\mathbf{x})=\hat{u}(\mathbf{x})-Q^{m+1}\hat{u}(\mathbf{x}). \tag{26}$$

Therefore, for a given point $\mathbf{x}_i$ we have

$$\hat{u}(\mathbf{x}_i)=Q^{m+1}\hat{u}(\mathbf{x}_i)+R^{m+1}\hat{u}(\mathbf{x}_i). \tag{27}$$

Substituting Eq. (27) into Eq. (22)

$$u^a(\mathbf{x}) = \sum_{i=1}^{NP} N_i(\mathbf{x})\hat{u}(\mathbf{x}_i) = \sum_{i=1}^{NP} N_i(\mathbf{x})Q^{m+1}\hat{u}(\mathbf{x}_i) + \sum_{i=1}^{NP} N_i(\mathbf{x})R^{m+1}\hat{u}(\mathbf{x}_i). \tag{28}$$

From the consistency conditions [10],

$$\begin{aligned}\sum_{i=1}^{NP} N_i(\mathbf{x})Q^{m+1}\hat{u}(\mathbf{x}_i) &= \sum_{i=1}^{NP} N_i(\mathbf{x}) \int_{B_j} \sum_{|\alpha|\leqslant m} \frac{(\mathbf{x}_i - \mathbf{y})^\alpha}{\alpha!} D^\alpha \hat{u}(\mathbf{y})\phi(\mathbf{y})\,\mathrm{d}\mathbf{y} \\ &= \int_{B_j} \sum_{|\alpha|\leqslant m} \frac{(\mathbf{x} - \mathbf{y})^\alpha}{\alpha!} D^\alpha \hat{u}(\mathbf{y})\phi(\mathbf{y})\,\mathrm{d}\mathbf{y} = Q^{m+1}\hat{u}(\mathbf{x}).\end{aligned} \tag{29}$$

Therefore,

$$u^a(\mathbf{x}) - \hat{u}(\mathbf{x}) = Q^{m+1}\hat{u}(\mathbf{x}) - \hat{u}(\mathbf{x}) + \sum_{i=1}^{NP} N_i(\mathbf{x})R^{m+1}\hat{u}(\mathbf{x}_i) = \sum_{i=1}^{NP} N_i(\mathbf{x})R^{m+1}\hat{u}(\mathbf{x}_i) - R^{m+1}\hat{u}(\mathbf{x}). \tag{30}$$

Assuming the domain boundary $\partial\Omega$ is Lipschitz continuous and smooth enough, one can properly choose $B_j$ and $\Omega_j$ such that the chunkiness parameter of $\overline{\Omega}_j \cap \overline{\Omega}$ are uniformly bounded [17]. From the results of [20, Section 4.3], the Taylor series expansion residual is bounded by

$$\|R^{m+1}\|_{W^{l,p}(\Omega_j\cap\Omega)} \leqslant cr^{m+1-l}\|u\|_{W^{m+1-l,p}(\Omega_j\cap\Omega)} \quad 0 \leqslant l \leqslant m+1, \tag{31}$$

$$\|R^{m+1}\|_{L^\infty(\Omega_j\cap\Omega)} \leqslant cr^{m+1-d/p} \cdot \|u\|_{W^{m+1,p}(\Omega_j\cap\Omega)}, \tag{32}$$

where $d$ is the dimension. Following the proof of Theorem 4.8 in [17], we obtain

$$\|u^a(\mathbf{x}) - \hat{u}(\mathbf{x})\|_{W^{0,p}(\Omega)} \leqslant C \cdot r^{m+1} \cdot \|\hat{u}(\mathbf{x})\|_{W^{m+1,p}(\Omega)} \quad m \geqslant p. \tag{33}$$

Therefore, there exists a constant $0 < C < \infty$ such that

$$\|u^a(\mathbf{x}) - \hat{u}(\mathbf{x})\|_{H^0(\Omega)} \leqslant C \cdot r^{m+1} \cdot \|\hat{u}(\mathbf{x})\|_{H^{m+1}(\Omega)}. \qquad \square \tag{34}$$

Define function space

$$\hat{U}^e(\Omega) = \left\{ \hat{u}^e \middle| \hat{u}^e \in C^{m+1}(\overline{\Omega}) \cap H^{m+1}(\Omega) : u(\mathbf{x}) = \sum_{i=1}^{NP} N_i(\mathbf{x})\hat{u}^e(\mathbf{x}_i) \right\}, \tag{35}$$

where $u(\mathbf{x})$ is the exact function. From Theorem 2, it also follows that

$$u(\mathbf{x}) = \hat{u}^e(\mathbf{x}) + \sum_{i=1}^{NP} N_i(\mathbf{x})R^{m+1}\hat{u}^e(\mathbf{x}_i) - R^{m+1}\hat{u}^e(\mathbf{x}) \tag{36}$$

and

$$\|u(\mathbf{x}) - \hat{u}^e(\mathbf{x})\|_{H^0(\Omega)} \leqslant C \cdot r^{m+1} \cdot \|\hat{u}^e(\mathbf{x})\|_{H^{m+1}(\Omega)}. \tag{37}$$

### 4.4. Error estimates for fixed kernel point collocation

In the finite cloud method, point collocation is used to discretize the governing equations. The point collocation for a node $\mathbf{x}$ is given by

$$\mathscr{L}u^a(\mathbf{x}) = f(\mathbf{x}) \quad \mathbf{x} \in \Omega, \tag{38}$$

where $\mathscr{L}$ is a linear differential operator, $f$ is the source function and $\mathbf{x}$ is any node in the domain. If $\mathbf{x}$ is a boundary node, $\mathscr{L}$ and $f(\mathbf{x})$ are defined by either Dirichlet or Neumann boundary condition. Let $\Omega_i \in \Omega$, $i = 1, \ldots, N$ be the set of clouds with $\mathbf{x}_i$ as the center of the $i$th cloud and the union of all the clouds covers the domain, i.e.,

$$\bigcup_{i=1}^{NP} \Omega_i = \overline{\Omega}. \tag{39}$$

Substituting the fixed kernel approximation, the point collocation for node $\mathbf{x}_i$ gives

$$\mathscr{L}\sum_{i=1}^{NP} N_i(\mathbf{x})\hat{u}(\mathbf{x}_i) = \sum_{i=1}^{NP} \mathscr{L}N_i(\mathbf{x})\hat{u}(\mathbf{x}_i) = f(\mathbf{x}). \tag{40}$$

Eq. (40) can be rewritten in a matrix form,

$$\mathbf{K}\hat{\mathbf{u}} = \mathbf{f}, \tag{41}$$

where $\mathbf{K}$ is an $NP \times NP$ matrix, $\hat{\mathbf{u}}$ is the $NP \times 1$ unknown vector, and $\mathbf{f}$ is the $NP \times 1$ right hand side vector. From the matrix form of Eq. (22), the $\hat{\mathbf{u}}$ vector is given by

$$\mathbf{u}^{\mathbf{a}} = \mathbf{N}\hat{\mathbf{u}}, \tag{42}$$

where $\mathbf{N}$ is the matrix of approximation functions. Therefore

$$\mathbf{K}\mathbf{N}^{-1}\mathbf{u}^{\mathbf{a}} = \mathbf{f}. \tag{43}$$

**Theorem 3.** *Assume the weighting function $\phi \in C^0(\overline{\Omega})$, the highest order of the differential operator in Eq. (38) is $n$, the polynomial basis is complete to the $m$th order and the point distributions are regular. Assume $u(\mathbf{x}), \hat{u}^e(\mathbf{x}) \in C^{m+1}(\overline{\Omega}) \cap H^{m+1}(\Omega)$ and the point-wise overlap condition holds. The error estimate for the finite cloud method is given by*

$$\frac{\|\mathbf{u}^{\mathbf{a}} - \mathbf{u}\|}{\|\mathbf{u}^{\mathbf{a}}\|} \leqslant C_1 \cdot \mathrm{Cond}(\mathbf{K}\mathbf{N}^{-1}) \cdot r^{m-n+1} \frac{\|f\|_{H^{m-n+1}(\Omega)} + C_2\|u\|_{H^{m+1}(\Omega)} + C_3\|\hat{u}^e\|_{H^{m+1}(\Omega)}}{\|\mathbf{f}\|}, \tag{44}$$

*where $0 < C_1, C_2, C_3 < \infty$.*

**Proof.** In general, the linear differential operator in Eq. (38) can be written as

$$\mathscr{L} = \sum_{h=0}^{n} \xi_h \mathscr{L}^h, \tag{45}$$

where $h$ is the order of the differential operator, $\xi_h$ is the coefficient of the $h$th order differential operator and $n$ is the highest order of $\mathscr{L}$.

Replacing $\hat{u}(\mathbf{x}_i)$ by $\hat{u}^e(\mathbf{x}_i)$ on the left hand side of Eq. (40) and applying Eq. (36)

$$\begin{aligned}\sum_{i=1}^{NP}\mathscr{L}N_i(\mathbf{x})\hat{u}^e(\mathbf{x}_i) &= \sum_{i=1}^{NP}\mathscr{L}N_i(\mathbf{x})\left[u(\mathbf{x}_i)-\sum_{j=1}^{NP}N_j(\mathbf{x}_i)R^{m+1}\hat{u}^e(\mathbf{x}_j)+R^{m+1}\hat{u}^e(\mathbf{x}_i)\right]\\ &= \sum_{i=1}^{NP}\sum_{h=0}^{n}\xi_h\mathscr{L}^hN_i(\mathbf{x})u(\mathbf{x}_i)-\sum_{i=1}^{NP}\mathscr{L}N_i(\mathbf{x})\left[\sum_{j=1}^{NP}N_j(\mathbf{x}_i)R^{m+1}\hat{u}^e(\mathbf{x}_j)-R^{m+1}\hat{u}^e(\mathbf{x}_i)\right]\\ &= \sum_{i=1}^{NP}\sum_{h=0}^{n}\xi_h\mathscr{L}^hN_i(\mathbf{x})\left[Q^{m+1-n+h}u(\mathbf{x}_i)+R^{m+1-n+h}u(\mathbf{x}_i)\right]\\ &\quad-\sum_{i=1}^{NP}\mathscr{L}N_i(\mathbf{x})\left[\sum_{j=1}^{NP}N_j(\mathbf{x}_i)R^{m+1}\hat{u}^e(\mathbf{x}_j)-R^{m+1}\hat{u}^e(\mathbf{x}_i)\right].\end{aligned}\tag{46}$$

By applying the consistency conditions, we obtain

$$\begin{aligned}\sum_{i=1}^{NP}\mathscr{L}N_i(\mathbf{x})\hat{u}^e(\mathbf{x}_i) &= \sum_{h=0}^{n}\xi_h\mathscr{L}^hQ^{m+1-n+h}u(\mathbf{x})+\sum_{i=1}^{NP}\sum_{h=0}^{n}\xi_h\mathscr{L}^hN_i(\mathbf{x})R^{m+1-n+h}u(\mathbf{x}_i)\\ &\quad-\sum_{i=1}^{NP}\mathscr{L}N_i(\mathbf{x})\left[\sum_{j=1}^{NP}N_j(\mathbf{x}_i)R^{m+1}\hat{u}^e(\mathbf{x}_j)-R^{m+1}\hat{u}^e(\mathbf{x}_i)\right]\\ &= Q^{m+1-n}f(\mathbf{x})+\sum_{i=1}^{NP}\sum_{h=0}^{n}\xi_h\mathscr{L}^hN_i(\mathbf{x})R^{m+1-n+h}u(\mathbf{x}_i)\\ &\quad-\sum_{i=1}^{NP}\mathscr{L}N_i(\mathbf{x})\left[\sum_{j=1}^{NP}N_j(\mathbf{x}_i)R^{m+1}\hat{u}^e(\mathbf{x}_j)-R^{m+1}\hat{u}^e(\mathbf{x}_i)\right]\\ &= f(\mathbf{x})-R^{m+1-n}f(\mathbf{x})+\sum_{i=1}^{NP}\sum_{h=0}^{n}\xi_h\mathscr{L}^hN_i(\mathbf{x})R^{m+1-n+h}u(\mathbf{x}_i)\\ &\quad-\sum_{i=1}^{NP}\mathscr{L}N_i(\mathbf{x})\left[\sum_{j=1}^{NP}N_j(\mathbf{x}_i)R^{m+1}\hat{u}^e(\mathbf{x}_j)-R^{m+1}\hat{u}^e(\mathbf{x}_i)\right].\end{aligned}\tag{47}$$

Therefore, Eq. (47) can be rewritten as

$$\sum_{i=1}^{NP}\mathscr{L}N_i(\mathbf{x})\hat{u}^e(\mathbf{x}_i)=f(\mathbf{x})+\theta(\mathbf{x}).\tag{48}$$

The matrix form of Eq. (48) is given by

$$\mathbf{K}\hat{\mathbf{u}}^{\mathbf{e}}=\mathbf{f}+\boldsymbol{\theta},\tag{49}$$

where $\boldsymbol{\theta}$ is a $NP\times 1$ vector of the truncation error. Eq. (49) can be rewritten as

$$\mathbf{K}\mathbf{N}^{-1}\mathbf{u}=\mathbf{f}+\boldsymbol{\theta}.\tag{50}$$

Defining $\mathbf{A}=\mathbf{K}\mathbf{N}^{-1}$, Eqs. (43) and (50) can be rewritten as

$$\mathbf{A}\mathbf{u}^{\mathbf{a}}=\mathbf{f},\tag{51}$$

$$\mathbf{A}\mathbf{u}=\mathbf{f}+\boldsymbol{\theta}.\tag{52}$$

From matrix analysis [22],

$$\frac{\|\mathbf{u}^{\mathbf{a}}-\mathbf{u}\|}{\|\mathbf{u}^{\mathbf{a}}\|}\leqslant \mathrm{Cond}(\mathbf{A})\frac{\|\boldsymbol{\theta}\|}{\|\mathbf{f}\|}, \tag{53}$$

where

$$\begin{aligned}\theta(\mathbf{x}) &= -R^{m+1-n}f(\mathbf{x})+\sum_{i=1}^{NP}\sum_{h=0}^{n}\xi_h\mathscr{L}^h N_i(\mathbf{x})R^{m+1-n+h}u(\mathbf{x}_i)\\ &\quad -\sum_{i=1}^{NP}\mathscr{L}N_i(\mathbf{x})\left[\sum_{j=1}^{NP}N_j(\mathbf{x}_i)R^{m+1}\hat{u}^e(\mathbf{x}_j)-R^{m+1}\hat{u}^e(\mathbf{x}_i)\right].\end{aligned} \tag{54}$$

Since the highest order of the governing differential operator is $n\geqslant 1$, from Eq. (19), it follows that

$$\max_{1\leqslant i\leqslant NP}\|\mathscr{L}N_i(\mathbf{x})\|_\infty\leqslant\frac{c}{r^n}\quad 0<c<\infty. \tag{55}$$

By using Eqs. (20), (31), (32), (55), the triangle inequality, Eq. (54) gives

$$\begin{aligned}\|\theta(\mathbf{x})\|_{W^{l,p}(B_j\cap\Omega)} &\leqslant \|R^{m-n+1}f(\mathbf{x})\|_{W^{l,p}(B_j\cap\Omega)}+\sum_{i=1}^{NP}\sum_{h=0}^{n}|\xi_h|\cdot\|\mathscr{L}^hN_i(\mathbf{x})\|_{W^{l,p}(B_j\cap\Omega)}\|R^{m+1-n+h}u(\mathbf{x})\|_{L^\infty(B_j\cap\Omega)}\\ &\quad+\sum_{i=1}^{NP}\|\mathscr{L}N_i(\mathbf{x})\|_{W^{l,p}(B_j\cap\Omega)}\|R^{m+1}\hat{u}^e(\mathbf{x})\|_{L^\infty(B_j\cap\Omega)}\\ &\quad+\sum_{i=1}^{NP}\|\mathscr{L}N_i(\mathbf{x})\|_{W^{l,p}(B_j\cap\Omega)}\sum_{j=1}^{NP}\|N_j(\mathbf{x})\|_{L^\infty(B_j\cap\Omega)}\cdot\|R^{m+1}\hat{u}^e(\mathbf{x})\|_{L^\infty(B_j\cap\Omega)}\\ &\leqslant c_1\cdot r^{m-n+1-l}\|f(\mathbf{x})\|_{W^{m-n+1-l,p}(\Omega_j\cap\Omega)}+c_2\cdot\sum_{h=0}^{n}|\xi_h|\cdot r^{m-n+1-l}\|u(\mathbf{x})\|_{W^{m+1-n+h-l,p}(\Omega_j\cap\Omega)}\\ &\quad+c_3\cdot r^{m-n+1-l}\|\hat{u}(\mathbf{x})\|_{W^{m+1-l,p}(\Omega_j\cap\Omega)}\\ &\leqslant C_1'\cdot r^{m-n+1-l}\Big\{\|f(\mathbf{x})\|_{W^{m-n+1-l,p}(\Omega_j\cap\Omega)}+C_2'\cdot\|u(\mathbf{x})\|_{W^{m+1-l,p}(\Omega_j\cap\Omega)}\\ &\quad+C_3'\cdot\|\hat{u}^e(\mathbf{x})\|_{W^{m+1-l,p}(\Omega_j\cap\Omega)}\Big\},\end{aligned} \tag{56}$$

where $0\leqslant l\leqslant m+1$. Let $p=2$, with $(m+1)p>d$, we have

$$\|\boldsymbol{\theta}\|\leqslant C_1r^{m+1-n}\{\|f(\mathbf{x})\|_{H^{m-n+1}(\Omega)}+C_2\cdot\|u(\mathbf{x})\|_{H^{m+1}(\Omega)}+C_3\cdot\|\hat{u}^e(\mathbf{x})\|_{H^{m+1}(\Omega)}\}, \tag{57}$$

where $0<C_1,\ C_2,\ C_3<\infty$. Thus the error estimate for the finite cloud method is given by

$$\frac{\|\mathbf{u}^{\mathbf{a}}-\mathbf{u}\|}{\|\mathbf{u}^{\mathbf{a}}\|}\leqslant C_1\cdot\mathrm{Cond}(\mathbf{A})\cdot r^{m+n-1}\frac{\|f\|_{H^{m-n+1}(\Omega)}+C_2\|u\|_{H^{m+1}(\Omega)}+C_3\|\hat{u}^e\|_{H^{m+1}(\Omega)}}{\|\mathbf{f}\|}\quad 0<C_1,C_2,C_3<\infty. \tag{58}$$

□

**Remarks**

1. It is easy to prove, for elliptic problems, that the matrix **A** is diagonally dominant when the positivity conditions are satisfied. Therefore, the condition number of **A** is improved. The basic idea of satisfying the positivity conditions is to ensure that the final matrix is diagonally dominant and consequently, reduces the error bound of the numerical solution.

2. Error analysis indicates that the condition number of the final coefficient matrix **A** not only serves as a criteria for assessing the accuracy of the solution to the linear system but also directly influences the error bound for collocation based meshless methods.
3. $\|\boldsymbol{\theta}\|$ depends on the value of the approximation function and its derivatives, the spacing between the points, and the cloud size. When a quadratic polynomial basis ($m = 2$) is used for interior clouds with a uniform point distribution, due to the symmetry of the points inside the cloud, the third-order truncation errors in Eq. (58) are canceled out and $\|\boldsymbol{\theta}\|$ is reduced. Therefore, the numerical solution of a problem with uniform point distribution typically exhibits higher accuracy compared to the scattered point distribution case.

## 5. Ensuring the positivity conditions in 1D meshless approximations

In this section, we show that in 1D cases, regardless of the point distribution, the positivity conditions can always be satisfied by appropriately selecting a weighting function. For a one-dimensional domain with scattered point distribution, corresponding to a star point $x_j$, denoting

$$w_l h_l^k = \sum_{l=1}^{NP} w_l h_l^k \quad k \in \mathbb{N}, \tag{59}$$

where $NP$ is the total number of points in the domain, $h_l = x_l - x_j$ and $w_l$ is the weighting assigned for point $l$. The analytical solution for the approximation function $N_i(x_j)$ is given by

$$\begin{aligned} N_i(x_j) = &-\frac{(w_l h_l^3)^2 - (w_l h_l^2)(w_l h_l^4)}{A} w_i + \frac{(w_l h_l^2)(w_l h_l^3) - (w_l h_l)(w_l h_l^4)}{A} w_i \cdot h_i \\ &- \frac{(w_l h_l^2)^2 - (w_l h_l)(w_l h_l^3)}{A} w_i \cdot h_i^2, \end{aligned} \tag{60}$$

where

$$A = -(w_l h_l^2)^3 + 2(w_l h_l)(w_l h_l^2)(w_l h_l^3) - (w_l h_l^0)(w_l h_l^3)^2 - (w_l h_l)^2 (w_l h_l^4) + (w_l h_l^0)(w_l h_l^2)(w_l h_l^4). \tag{61}$$

The first-order derivative of the approximation function is given by

$$\begin{aligned} \frac{\partial N_i(x_j)}{\partial x} = &\frac{(w_l h_l^2)(w_l h_l^3) - (w_l h_l)(w_l h_l^4)}{A} w_i - \frac{(w_l h_l^2)^2 - (w_l h_l^0)(w_l h_l^4)}{A} w_i \cdot h_i \\ &+ \frac{(w_l h_l)(w_l h_l^2) - (w_l h_l^0)(w_l h_l^3)}{A} w_i \cdot h_i^2 \end{aligned} \tag{62}$$

and the second-order derivative of the approximation function is given by

$$\begin{aligned} \frac{\partial^2 N_i(x_j)}{\partial x^2} = &-2\frac{(w_l h_l^2)^2 - (w_l h_l)(w_l h_l^3)}{A} w_i + 2\frac{(w_l h_l)(w_l h_l^2) - (w_l h_l^0)(w_l h_l^3)}{A} w_i \cdot h_i \\ &- 2\frac{(w_l h_l)^2 - (w_l h_l^0)(w_l h_l^2)}{A} w_i \cdot h_i^2. \end{aligned} \tag{63}$$

Eqs. (60), (62), (63) show that the value of the approximation function and its derivatives are determined by the weighting function and the point distribution. Given a set of points, one can construct a weighting function to satisfy the positivity conditions. Defining the coefficients

$$a = -(w_l h_l)^2 + (w_l h_l^0)(w_l h_l^2), \tag{64}$$

$$b = -(w_l h_l)(w_l h_l^2) + (w_l h_l^0)(w_l h_l^3), \tag{65}$$

$$c = (w_l h_l^2)^2 - (w_l h_l)(w_l h_l^3). \tag{66}$$

The second derivative of the approximation function can be rewritten as

$$\frac{\partial^2 N_i(x_j)}{\partial x^2} = -\frac{2c}{A} w_i - \frac{2b}{A} w_i h_i + \frac{2a}{A} w_i h_i^2. \tag{67}$$

It is easy to show that $a > 0$ and $c > 0$. As shown in Appendix A, the meshless approximation function satisfies the first positivity condition (Eq. (8)), if and only if it has the Kronecker delta property. In meshless approximations, there are various ways to satisfy the first positivity condition [23–26]. In the fixed kernel approximation, the approximation would possess the Kronecker delta property if the weighting function behaves like a delta function. Therefore, it is better to chose a weighting function such that the value of the weighting function at the star point is much higher compared to the value at the other nodes in the cloud. Therefore, coefficient $A$ in Eq. (67) is greater than zero. In this case, it is obvious that, when $h_i = 0$, $\frac{\partial^2 N_i(x_j)}{\partial x^2} < 0$. Thus, the third positivity condition (Eq. (10)) is automatically satisfied. For illustration purpose, we choose a weighting function such that $w_j \gg w_i$, for $i \neq j$, where $w_j$ is the value of the weighting function at the star point $x_j$. A class of weighting functions which seem to be a good choice are of the form

$$w_i = \frac{1}{|h_i|^r + \epsilon} \eta_i, \tag{68}$$

where $r$ is the order of the weighting, $\eta_i$ is the nodal coefficient for point $i$, $\epsilon$ is a small value to avoid the singularity at the star point ($\epsilon \ll |h_i|^r$, for $i \neq j$). It is easy to show that the approximation function possesses the Kronecker delta property as $w_j \to \infty$ corresponding to $\epsilon \to 0$. By choosing a sufficiently small $\epsilon$, e.g., $10^{-5} \times \min\{|h_i|^r, i \neq j\}$, one can get

$$N_i(x_j) \approx \begin{cases} 1 & i = j, \\ 0 & i \neq j. \end{cases} \tag{69}$$

Thus, it is reasonable to say that the first positivity condition can be satisfied by choosing a sufficiently small $\epsilon$. The rest of the analysis will focus on the second positivity condition (Eq. (9)). Since $w_j \gg w_i$, for $i \neq j$, the positivity condition for Eq. (63) can be simplified as

$$\sum_{l=1}^{NP} w_l h_l^2 h_i (h_i - h_l) > 0 \tag{70}$$

i.e., Eq. (63) satisfies the second positivity condition if Eq. (70) holds. It can be shown that, if all the points in a cloud lie on one side of the star node, the left handside of Eq. (70) is negative at the point closest to the star node. Thus, the second positivity condition is violated. Therefore, to satisfy the second positivity condition, there must be at least one point on either side of the star node. This condition must be enforced as a rule in determining the cloud for each point.

The left hand side of Eq. (70) is a quadratic function of $h_i$. Since the second derivative of the approximation function for the star node ($h_i = 0$) is negative (this is the third positivity condition given in Eq. (10)), the second positivity condition shown in Eq. (70) is more likely to be violated at the points closest to the star node. Therefore, the second derivative of the approximation function at the nearest point on each side of the star node is studied. A typical cloud in a one-dimensional case is shown in Fig. 4. Denoting the star node as $x_0$ and the nodes on the right and the left hand sides of the star node as $x_1, x_2, \ldots, x_m$ and $x_{-1}, x_{-2}, \ldots, x_{-n}$, respectively, where $m$ and $n$ are the number of nodes on each side of the star node. The second positivity condition of the points $x_1$ and $x_{-1}$ can be rewritten as

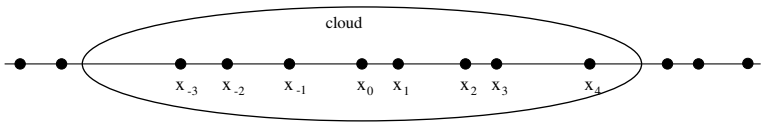


Fig. 4. A cloud in one-dimensional case. $x_0$ is the star node. $x_1$, $x_2$, $x_3$, and $x_4$ are the right hand side nodes in the cloud of $x_0$. $x_{-1}$, $x_{-2}$, and $x_{-3}$ are the left hand side nodes in the cloud of $x_0$.

$$\sum_{l=-1}^{-n} w_l h_l^2 h_1(|h_1| + |h_l|) - \sum_{l=1}^{m} w_l h_l^2 h_1(|h_l| - |h_1|) > 0, \tag{71}$$

$$\sum_{l=-1}^{-n} w_l h_l^2 h_{-1}(|h_l| - |h_{-1}|) - \sum_{l=1}^{m} w_l h_l^2 h_{-1}(|h_l| + |h_{-1}|) > 0. \tag{72}$$

It is obvious that when the order of the weighting is $r = 3$ (see Eq. (68)), and if we let the nodal coefficient of the weighting function $\eta_l = n$ for $l = 1, 2, \ldots, m$ and $\eta_l = m$ for $l = -1, -2, \ldots, -n$, Eqs. (71) and (72) are satisfied, i.e., the second positivity condition holds for $x_1$ and $x_{-1}$, which are the nearest to the star node on either side. It can be easily shown that if the second positivity condition holds for $x_1$ and $x_{-1}$, it must be satisfied at the rest of the nodes in the cloud. For the example shown in Fig. 4, if we assign the nodal weighting coefficient to be 3 for all the nodes on the right hand side of the star node and 4 for all the left hand side nodes, then the second positivity condition is satisfied. In this paper, the weighting function given in Eq. (68) with $r = 3$ is denoted as cubic inverse distance weighting. Note that when $r \neq 3$, a more complicated algorithm is necessary to compute the nodal coefficient $\eta_i$ so that the second positivity condition is satisfied.

## 6. Positivity conditions in 2D meshless approximations

In 1D meshless approximations, one can compute the weight for each point within a cloud so that the positivity conditions can be satisfied. However, in two-dimensions, given a scattered set of points, it is more difficult to ensure that the second positivity condition is satisfied. The difficulty arises from the posibility that, within a cloud, the points may be "badly" distributed, i.e., the center of the point distribution in the cloud deviates severely from the star point. For these ill-balanced clouds, the positivity conditions are more likely to be violated. Qualitative criteria have been proposed in the literature [9] to measure the quality of a cloud (star). However, in numerical implementation, quantitative criteria are needed to check the quality of a cloud.

There are three options to investigate the positivity conditions in 2D: (1) within the framework of kernel/least-squares approximations, enforce the point distribution within a cloud to satisfy a set of quantitative criteria for a given weighting function to guarantee the satisfaction of the positivity conditions, (2) reduce the negative values of $\nabla^2 N_i(\mathbf{x}_j)$, $i \neq j$ as much as possible so that positivity conditions are not violated too badly or (3) use a different framework that is not based on kernel/least-squares approximations. In this paper, we discuss the first and the second approaches.

For the first approach, since the value of the approximation function and its derivatives is a function of the weighting and the spacing among the points within the cloud, given a weighting function, one can develop quantitative criteria to find "bad" clouds and redefine the clouds so that the positivity conditions are satisfied. Appendix B shows the derivation of a set of quantitative criteria for the weighting function of the form

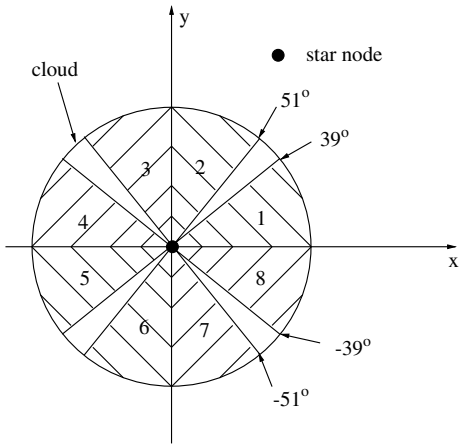


Fig. 5. Eight sectors in a two-dimensional cloud which are divided by 39° and 51° lines.

$$w_i = \frac{1}{r_i^4 + \epsilon}, \tag{73}$$

where $r_i = |\mathbf{x}_i - \mathbf{x}_j|$ is the distance from point $\mathbf{x}_i$ to the star point $\mathbf{x}_j$. For other weighting functions, using the approach presented in Appendix B, it is possible to derive mathematical criteria to satisfy the positivity conditions. Given a star point and the weighting function in Eq. (73), the following steps can be implemented to define clouds that satisfy positivity conditions:

**Algorithm 1**

1. *Step 1:* Select the points of the cloud. In order to get a well balanced cloud, one needs to select the same number of points in each of the eight shaded sectors of the cloud, as shown in Fig. 5 (see Appendix B for details).
2. *Step 2:* Check the regularity of the cloud. If the moment matrix $M$ (Eq. (5)) is singular or ill conditioned, the cloud is taken to be a "bad" cloud. In this case, more points need to be included in the cloud.
3. *Step 3:* Check the quality of the cloud for positivity conditions. Assuming that the star node of the cloud is $(x_j, y_j)$, the nodes inside the cloud are denoted by $(x_i, y_i)$ $(i = 1, 2, \ldots)$ and

$$\begin{aligned} hx_i &= x_i - x_j, \\ hy_i &= y_i - y_j. \end{aligned} \tag{74}$$

The criterion for a good quality cloud to satisfy the positivity conditions (see Appendix B) is given by

$$\min\left(\sum_i w_i hx_i^2, \sum_i w_i hy_i^2\right) \gg \max\left(\sum_i w_i hx_i hy_i, \frac{\sum_i w_i hx_i \sum_i w_i hy_i}{\sum_i w_i}\right),$$

$$\min\left(\sum_i w_i hx_i^4, \sum_i w_i hx_i^2 hy_i^2, \sum_i w_i hy_i^4\right) \gg \max\left(\sum_i w_i hx_i^3 hy_i, \sum_i w_i hx_i hy_i^3\right). \tag{75}$$

If Eq. (75) does not hold for the cloud, the cloud is taken to be a "bad" cloud. Typically, including more points in the cloud can enable a cloud to satisfy Eq. (75). However, this is not always guaranteed. In the extreme cases, the point distribution in the vicinity of the star point needs to be modified.

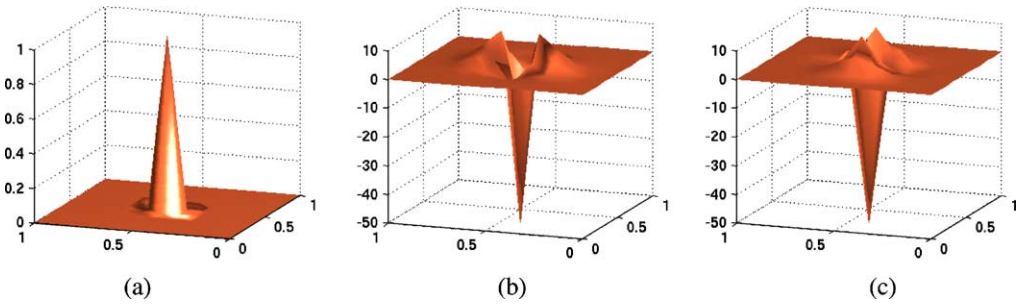


Fig. 6. 2D fixed kernel approximation function and its derivatives: (a) $N(x,y)$, (b) $\partial^2 N(x,y)/\partial x^2$, (c) $\partial^2 N(x,y)/\partial y^2$.

4. *Step 4:* Compute the fixed kernel approximations and the derivatives by using the selected points within each cloud.

Alternatively, one can adopt the second approach, i.e., try to reduce the negative values of $\nabla^2 N_i(\mathbf{x}_j)$, $i \neq j$ as much as possible. We have found that the 2D version of the cubic inverse weighting function given in Eq. (68) and a modified Gaussian weighting function are good choices, i.e., even if the positivity conditions are violated, the deviation is small with these weighting functions. The cubic inverse distance weighting function and the modified Gaussian weighting function in 2D are given by

$$w_i(x_j, y_j) = \frac{1}{r_i^3 + \epsilon}\eta_i \tag{76}$$

and

$$w_i(x_j, y_j) = \frac{\phi(x_i - x_j)}{1 - \phi(x_i - x_j) + \epsilon} \times \frac{\phi(y_i - y_j)}{1 - \phi(y_i - y_j) + \epsilon}, \tag{77}$$

where $r_i = |\mathbf{x}_i - \mathbf{x}_j|$ is the distance from point $\mathbf{x}_i$ to the star point $\mathbf{x}_j$, $\phi(x_i - x_j)$ is the Gaussian weighting function given in Eq. (15). The weighting function given in Eq. (77) is denoted as the modified Gaussian weighting. Note that the nodal coefficients $\eta_i$ in Eq. (68), can be computed by using the approach described in Section 5 to minimize the deviation from the positivity conditions in 2D. However, here the $\eta_i$s are taken to be 1 for the sake of simplicity. Fig. 6(a)–(c) show the fixed kernel approximation function and its derivatives by using the weighting function given in Eq. (77). As shown in the figures, the approximation function $N(x,y)$ is very close to the Kronecker delta function and the positivity conditions on the second derivatives are satisfied.

## 7. Numerical results

In this section, 1D and 2D numerical examples are presented to demonstrate the significance of the positivity conditions. Section 7.1 shows a 1D example where the approach described in Section 5 is used for ensuring the positivity conditions. The results obtained by satisfying the positivity conditions have been compared with those that do not satisfy the positivity conditions (i.e., using the classical Gaussian weighting). Sections 7.2–7.4 present several 2D problems with scattered point distributions. Weighting functions given in Eqs. (73), (76), (77) are used for 2D calculations. The results are compared with those

obtained with the 2D version of the classical Gaussian weighting (Eq. (15)). The error in the solution is computed by using Eq. (16).

### 7.1. Example in 1D

A set of randomly generated one-dimensional scattered points is shown in Fig. 7. 32 points are used in this example. The cloud of each node includes the closest 7 points. Fig. 8 shows the approximation functions obtained by using the regular Gaussian weighting function (Eq. (15)) and the cubic inverse distance weighting function. The positivity condition (Eq. (8)) is violated when the regular Gaussian weighting function is used while it is satisfied by using the new weighting. Fig. 9 shows the second-derivative of the approximation function when the regular Gaussian weighting function and the new weighting function are used. The violation of the positivity condition (Eq. (9)) is eliminated by using the new weighting function. The effectiveness of the new weighting function and the approach described in Section 5 is clearly shown in this example.

The set of scattered points are further used to solve the 1D Poisson problem given in Eq. (13). Fig. 10 shows the FCM solution with different weighting functions. Since the positivity conditions do not hold for the regular Gaussian weighting function, the error in the solution is quite large. But the solutions with the new weighting function match well with the exact solution.

Numerical properties of the FCM including the condition number of the final coefficient matrix, the third order truncation error and the error in the solution obtained from different weighting functions are summarized in Tables 1 and 2. As shown in Tables 1 and 2, the condition number of the matrix is much

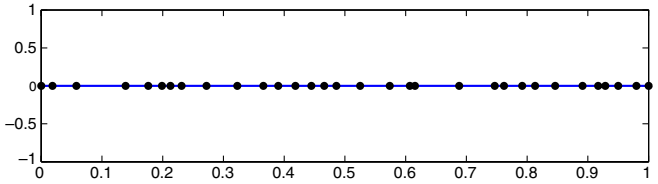


Fig. 7. Scattered point distribution in one-dimension.

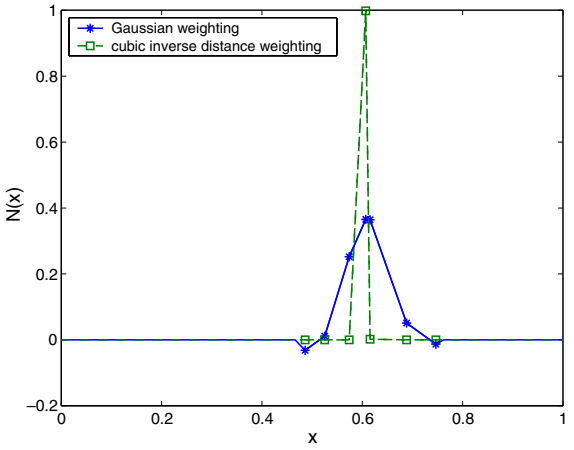


Fig. 8. Approximation function for the point at $x = 0.6$.

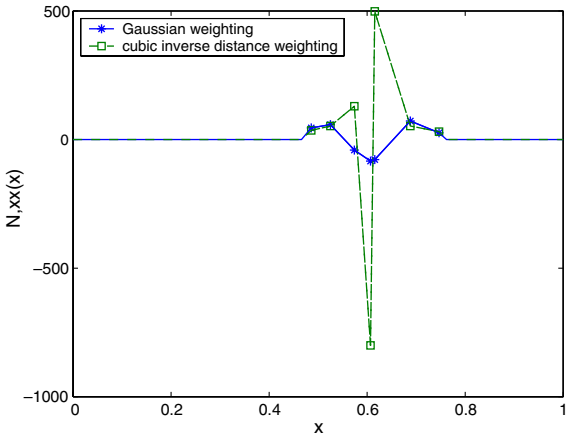


Fig. 9. Second derivative of the approximation function for the point at $x = 0.6$.

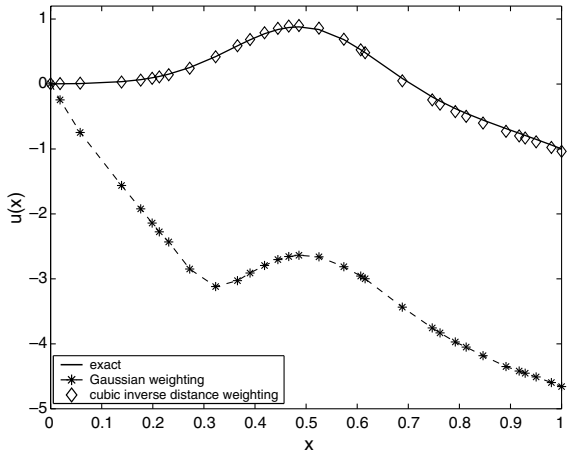


Fig. 10. Comparison of the exact solution and the computed results by using different weighting functions.

Table 1
Numerical properties with the regular Gaussian weighting function

| Cloud size | 7 Points | 9 Points | 13 Points |
|---|---|---|---|
| Cond($K$) | $1.6\times10^{7}$ | $6.7\times10^{5}$ | $1.7\times10^{8}$ |
| Solution error | 3.2 | 0.37 | 4.8 |

Table 2
Numerical properties with the new weighting function given in Eq. (68)

| Cloud size | 7 Points | 9 Points | 13 Points |
|---|---|---|---|
| Cond($K$) | $2.5\times10^{5}$ | $1.3\times10^{5}$ | $5.1\times10^{4}$ |
| Solution error | 0.027 | 0.033 | 0.04 |

smaller when the new weighting function is used. Consequently, from the error analysis, the error in the solution for the new weighting function is much smaller. We have also observed that the FCM solution is less sensitive to the cloud size with the new weighting function.

### 7.2. 2D Poisson equation

A two-dimensional extension of the 1D Poisson example is considered. The governing equation along with the boundary conditions are given by

$$\frac{\partial^2 u}{\partial x^2}+\frac{\partial^2 u}{\partial y^2}=-6x-6y-\left[\frac{4}{\alpha^2}-4\left(\frac{x-\beta}{\alpha^2}\right)^2-4\left(\frac{y-\beta}{\alpha^2}\right)^2\right]\times\exp\left[-\left(\frac{x-\beta}{\alpha}\right)^2-\left(\frac{y-\beta}{\alpha}\right)^2\right]\quad 0\leqslant x\leqslant 1\quad 0\leqslant y\leqslant 1, \tag{78}$$

$$u(x=0)=-y^3+\exp\left[-\left(\frac{\beta}{\alpha}\right)^2-\left(\frac{y-\beta}{\alpha}\right)^2\right], \tag{79}$$

$$u(y=0)=-x^3+\exp\left[-\left(\frac{x-\beta}{\alpha}\right)^2-\left(\frac{\beta}{\alpha}\right)^2\right], \tag{80}$$

$$u_{,x}(x=1)=-3-2\left(\frac{1-\beta}{\alpha^2}\right)\exp\left[-\left(\frac{1-\beta}{\alpha}\right)^2-\left(\frac{y-\beta}{\alpha}\right)^2\right], \tag{81}$$

$$u_{,y}(y=1)=-3-2\left(\frac{1-\beta}{\alpha^2}\right)\exp\left[-\left(\frac{x-\beta}{\alpha}\right)^2-\left(\frac{1-\beta}{\alpha}\right)^2\right], \tag{82}$$

where $\alpha=0.2$ and $\beta=0.5$. The exact solution for this problem is given by

$$u=-x^3-y^3+\exp\left[-\left(\frac{x-\beta}{\alpha}\right)^2-\left(\frac{y-\beta}{\alpha}\right)^2\right]. \tag{83}$$

Fig. 11 shows a $1\times1$ square domain with an irregular scattered point distribution. There are 455 points sprinkled over the domain. Fig. 12 shows a comparison of the solutions along the line $x=1$. Fig. 13 shows a comparison of the computed and the exact solution for the $y$-derivative along $x=1$. 20 point clouds are used for all the three cases. FCM gives a good solution when the positivity conditions are satisfied by using the quartic inverse distance weighting function, while in the case of the regular Gaussian weighting function inaccurate results are obtained. The cubic inverse distance weighting and the modified Gaussian weighting also give quite good results. Table 3 shows the comparison of the errors when different cloud sizes are used. We have also observed that the FCM solution is less sensitive to the cloud size with the quartic inverse distance weighting function.

The Poisson problem in Eq. (78) is also solved by employing a random distribution of 81, 289 and 1089 points to show the convergence of the method with different weighting functions. The point distributions are shown in Figs. 14–16. The convergence plots for the cloud sizes of 16 and 20 points are shown in Figs. 17 and 18. We have observed that the convergence is affected significantly by the cloud size when the regular Gaussian weighting is used.

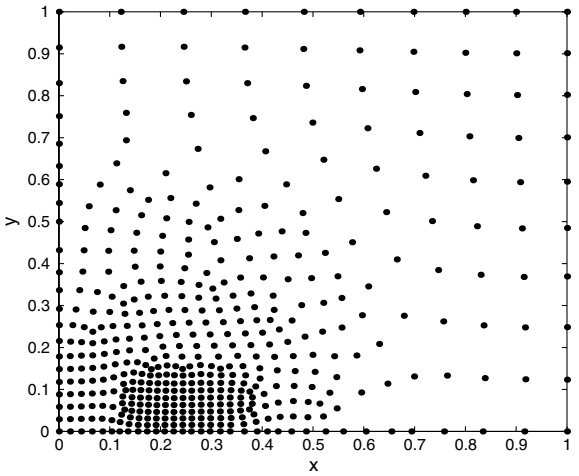


Fig. 11. Scattered point distribution over a square domain.

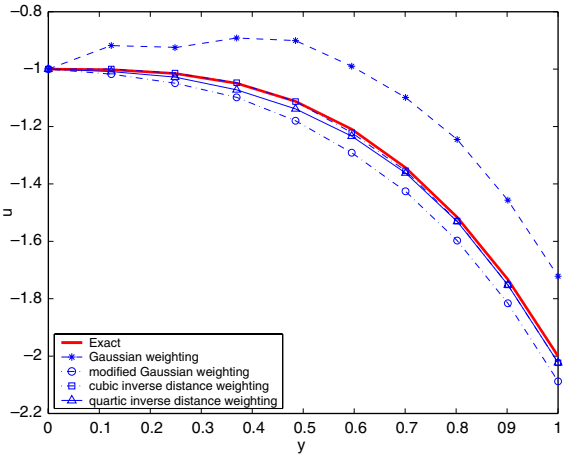


Fig. 12. Comparison of the exact solution and the computed results along $x = 1$.

### 7.3. 2D elasticity: beam bending

A $1\times1$ beam subjected to a uniform load and a shear as shown in Fig. 19 is considered. The beam is centered at $(a, b) = (0.5, 0.5)$, $l = 0.5$ unit, $c = 0.5$ and $t = 1$ unit. The modulus of elasticity is $3 \times 10^7$ and the Poisson's ratio is 0.25.

The governing equations for elasticity (in a plane stress situation) are

$$\frac{2}{1-v}\frac{\partial^2 u}{\partial x^2}+\frac{1+v}{1-v}\frac{\partial^2 v}{\partial x y}+\frac{\partial^2 u}{\partial y^2}=0, \tag{84}$$

$$\frac{2}{1-v}\frac{\partial^2 v}{\partial y^2}+\frac{1+v}{1-v}\frac{\partial^2 u}{\partial x y}+\frac{\partial^2 v}{\partial x^2}=0, \tag{85}$$

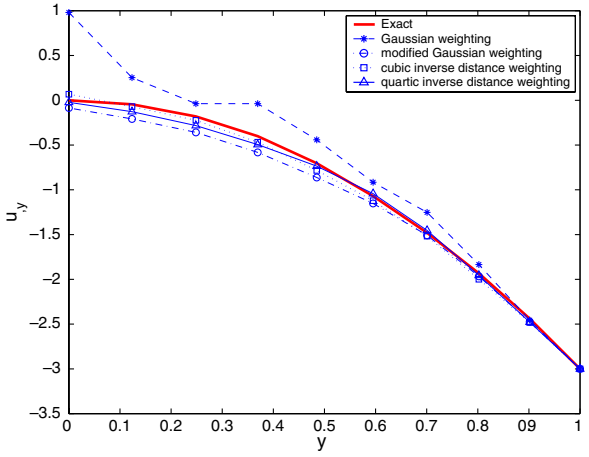


Fig. 13. Comparison of the exact solution and the computed results for the $y$-derivative along $x = 1$.

Table 3
Errors for the 2D Poisson problem by using the regular Gaussian weighting function and the quartic inverse distance weighting function

| Cloud size | 20 Points | 25 Points | 30 Points |
|---|---|---|---|
| Gaussian weighting function | 0.034 | 0.12 | 0.28 |
| Quartic inverse distance weighting function | 0.013 | 0.02 | 0.019 |

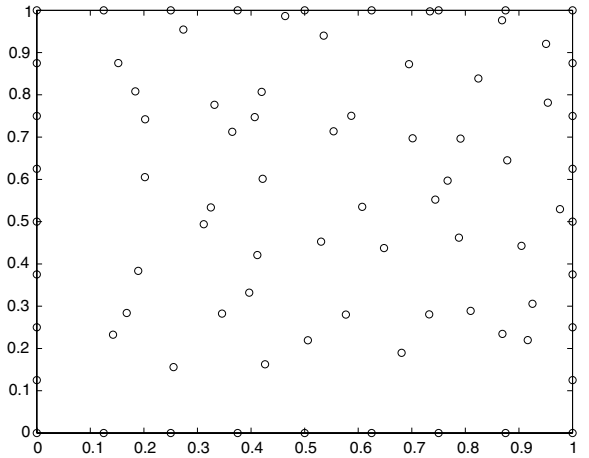

Fig. 14. 2D domain with 81 random points.

where $u$ and $v$ are the $x$- and $y$-components of the displacement and $v$ is the Poisson's ratio. The boundary conditions are given by

$$u(x = a + l, y = b) = \frac{vql}{2E},$$

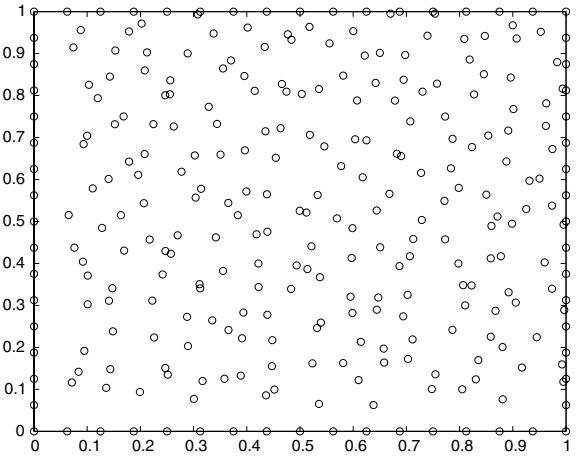


Fig. 15. 2D domain with 289 random points.

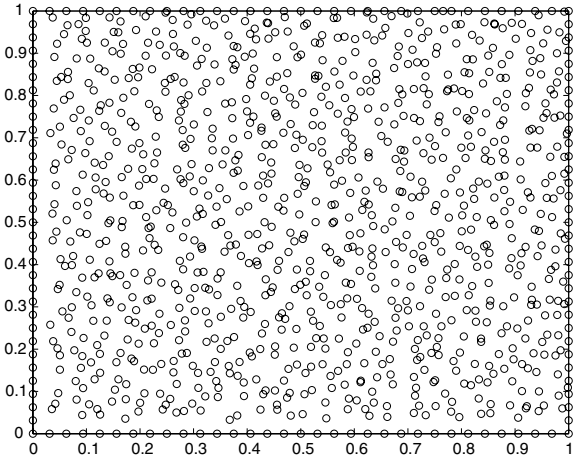


Fig. 16. 2D domain with 1089 random points.

$$v(x = a \pm l, y = b) = 0,$$

$$\tau_{xy}(y = b \pm c) = 0,$$

$$\sigma_y(y = b - c) = -q,$$

$$\sigma_y(y = b + c) = 0,$$

$$\sigma_x(x = a \pm l) = \frac{q}{2I}\left[\frac{2}{3}(y-b)^3 - \frac{2}{5}c^2(y-b)\right],$$

$$\tau_{xy}(x = a \pm l) = -\frac{q}{2I}(x-a)[c^2 - (y-b)^2].$$

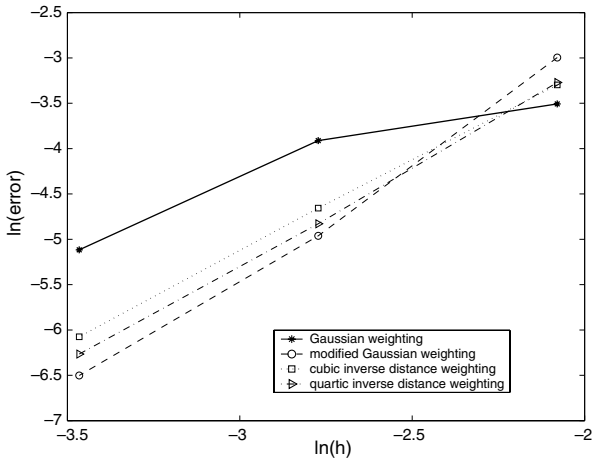


Fig. 17. Convergence plot with different weighting functions when the cloud size is 16.

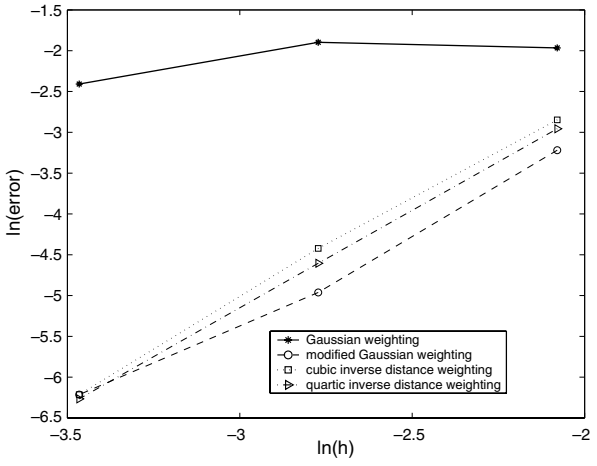


Fig. 18. Convergence plot with different weighting functions when the cloud size is 20.

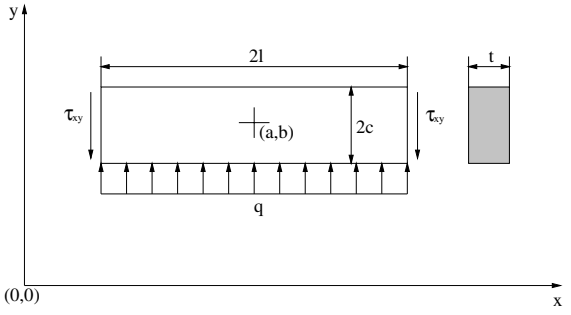


Fig. 19. Beam subjected to a uniform load and a shear.

The exact solution for this problem is given by [27]

$$u = \frac{q}{2EI}\left\{\left[l^2(x-a) - \frac{(x-a)^3}{3}\right](y-b) + (x-a)\left[\frac{2}{3}(y-b)^3 - \frac{2}{5}c^2(y-b)\right] + v(x-a)\left[\frac{(y-b)^3}{3} - c^2(y-b) + \frac{2}{3}c^3\right]\right\}, \tag{86}$$

$$v = -\frac{q}{2EI}\left\{\frac{(y-b)^4}{12} - \frac{c^2(y-b)^2}{2} + \frac{2c^3(y-b)}{3} + v\left[(l^2-(x-a)^2)\frac{(y-b)^2}{2} + \frac{(y-b)^4}{6} - \frac{c^2(y-b)^2}{5}\right]\right\} - \frac{q}{2EI}\left[\frac{l^2(x-a)^2}{2} - \frac{(x-a)^4}{12} - \frac{c^2(x-a)^2}{5} + \left(1+\frac{1}{2}v\right)c^2(x-a)^2\right] + \delta, \tag{87}$$

$$\delta = \frac{5}{24}\frac{ql^4}{EI}\left[1 + \frac{12}{5}\frac{c^2}{l^2}\left(\frac{4}{5} + \frac{v}{2}\right)\right]. \tag{88}$$

The scattered point distribution shown in Fig. 11 is used to solve the beam bending problem. Regular Gaussian weighting function, the cubic and quartic inverse distance weighting functions are used. In all cases, 20-point clouds are used. The $x$- and $y$-displacements along $x = 0$ are shown in Figs. 20 and 21, respectively. As shown in Figs. 20 and 21, the regular Gaussian weighting function gives poor results. The quartic and cubic inverse distance weighting functions give good results. The condition number of the final matrix is again observed to be improved by using the inverse distance weighting functions. Table 4 shows the comparison of the errors for different cloud sizes when the regular Gaussian weighting function and the quartic inverse distance weighting function are used. We again observed that the FCM solution is less sensitive to the cloud size with the quartic inverse distance weighting function.

### 7.4. 2D elasticity: plate with a hole

The second elasticity example is an infinite plate with a central circular hole subjected to a unit radial tensile load. Due to the symmetry, only the first quadrant of the plate is considered as shown in Fig. 22.

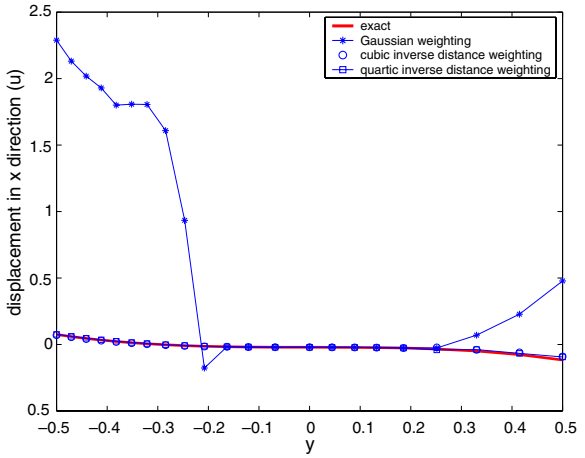


Fig. 20. Comparison of the exact and the computed $x$-displacement along $x = 0$ for the beam bending problem.

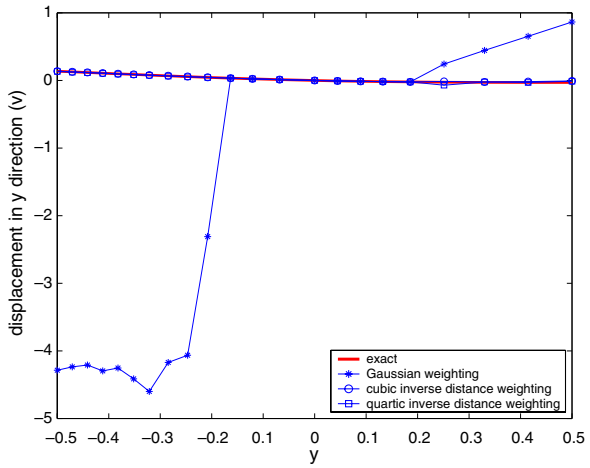


Fig. 21. Comparison of the exact and the computed $y$-displacement along $x = 0$ for the beam bending problem.

Table 4
Errors in the $x$-displacement for the 2D bending beam problem when the regular Gaussian weighting function and the quartic inverse distance weighting function are used

| Cloud size | 12 Points | 16 Points | 20 Points |
|---|---|---|---|
| Gaussian weighting function | 0.2 | 0.6 | 0.33 |
| Quartic inverse distance weighting function | 0.01 | 0.02 | 0.03 |

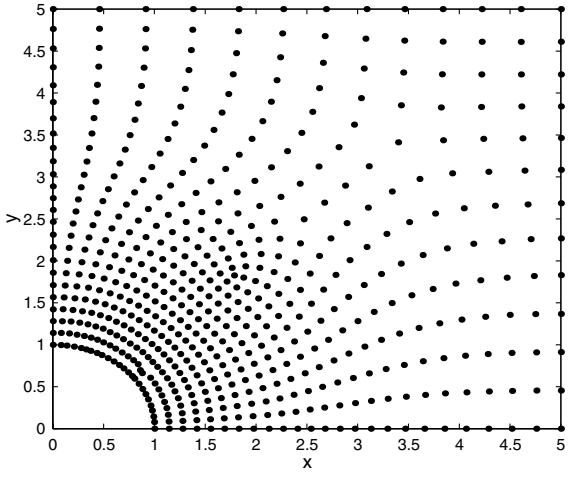


Fig. 22. Scattered point distribution for the plate-with-a-hole problem.

Symmetric boundary conditions were imposed on the left and bottom edges, and the inner circle boundary of radius 1 is traction-free. The modulus of elasticity is taken as $1.0\times10^3$ and the Poisson ratio is 0.3. The exact solution for the stresses is given by

$$\sigma_x(x,y) = 1 - \frac{a^2}{r^2}\left[\frac{3}{2}\cos 2\theta + \cos 4\theta\right] + \frac{3a^4}{2r^4}\cos 4\theta, \tag{89}$$

$$\sigma_y(x,y) = -\frac{a^2}{r^2}\left[\frac{1}{2}\cos 2\theta - \cos 4\theta\right] - \frac{3a^4}{2r^4}\cos 4\theta, \tag{90}$$

$$\sigma_{xy}(x,y) = -\frac{a^2}{r^2}\left[\frac{1}{2}\sin 2\theta + \sin 4\theta\right] + \frac{3a^4}{2r^4}\sin 4\theta. \tag{91}$$

The scattered point distribution for this example is shown in Fig. 22. 20 point clouds are used for this example. Fig. 23 compares the exact solution and the results obtained by using the regular Gaussian weighting, the quartic and cubic inverse distance weighting and the modified Gaussian weighting for the stress $\sigma_x$ along $x = 0$. The reduction in the condition number of the final matrix by using the new weighting functions is again observed. The large error exhibited with the regular Gaussian weighting function is eliminated by using the inverse distance weighting functions. Table 5 shows the comparison of the errors when different cloud sizes are used. The results show that the quartic inverse distance weighting function provides a superior performance over the regular Gaussian weighting function.

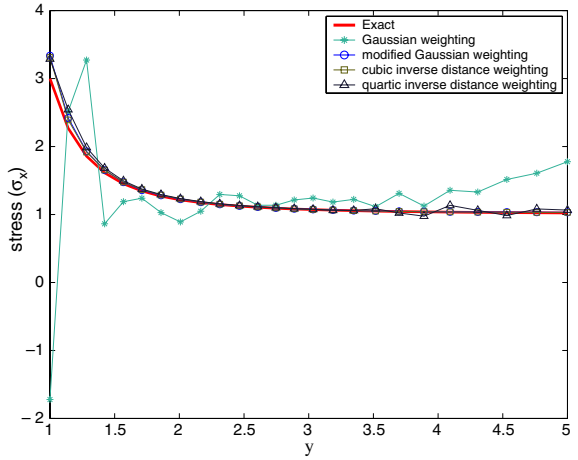


Fig. 23. Comparison of $\sigma_x$ along $x = 0$ obtained by Gaussian, cubic inverse distance, quartic inverse distance and modified Gaussian weighting functions with the exact solution.

Table 5
Errors in $\sigma_x$ for the plate-with-a-hole problem by using the regular Gaussian weighting function and the quartic inverse distance weighting function

| Cloud size | 16 Points | 20 Points | 24 Points |
|---|---|---|---|
| Gaussian weighting function | 0.36 | 0.11 | 0.02 |
| Quartic inverse distance weighting function | 0.04 | 0.0098 | 0.007 |

## 8. Conclusion

In this paper, we have shown the significance of the positivity conditions in meshless collocation approaches. From an error analysis of the finite cloud method, we have shown that the error bound of the numerical solution is directly related to the condition number of the final coefficient matrix. Violation of the positivity conditions can significantly increase the condition number resulting in a large error in the numerical solution. Satisfying the positivity conditions ensures that the final coefficient matrix is diagonally dominant. Consequently, the condition number of the final matrix and the error bound of the solution are reduced. For 1D boundary value problems, it is shown that for any given set of scattered points, the positivity conditions can always be satisfied by employing a weighting function of the form (see Eq. (68))

$$w_i = \frac{1}{|h_i|^r + \epsilon}\eta_i.$$

For 2D scattered point distributions, it is more difficult to satisfy the positivity conditions. We have employed three types of weighting functions: the cubic and quartic inverse distance weighting and the modified Gaussian weighting (see Eqs. (73), (76), (77))

$$w_i(x_j, y_j) = \frac{1}{r_i^4 + \epsilon} \quad w_i(x_j, y_j) = \frac{1}{r_i^3 + \epsilon}$$

and

$$w_i(x_j, y_j) = \frac{\phi(x_i - x_j)}{1 - \phi(x_i - x_j) + \epsilon} \times \frac{\phi(y_i - y_j)}{1 - \phi(y_i - y_j) + \epsilon}.$$

For the quartic inverse distance weighting function, we have shown that the positivity conditions can be satisfied by imposing requirements on the point distributions within the cloud. Alternatively, a simpler approach is to reduce the violation of the positivity conditions. We have found that the cubic inverse distance and the modified Gaussian weighting functions are good choices. Although the positivity conditions can be violated for certain clouds, the deviation is quite small with these weighting functions and satisfactory results are obtained. Finally, numerical results are presented for 1D and 2D problems to demonstrate the effectiveness of the positivity conditions in meshless collocation methods.

## Acknowledgements

This research was supported by the National Science Foundation under Grants CCR-9875671 and ACI-0217986. This support is gratefully acknowledged. The authors would like to thank the anonymous reviewers, whose comments have helped improve the paper.

## Appendix A. Positivity of the approximation function

In kernel or least-squares meshless approximation methods, the approximation of an unknown $u$ at a point $j$ can be written in a generalized form

$$u^a(\mathbf{x}_j) = \sum_i N_i(\mathbf{x}_j)\hat{u}(\mathbf{x}_i), \tag{A.1}$$

$$D^{\alpha}u^{a}(\mathbf{x}_j) = \sum_i D^{\alpha}N_i(\mathbf{x}_j)\hat{u}(\mathbf{x}_i), \tag{A.2}$$

where $\hat{u}(\mathbf{x}_i)$ is the unknown at point $j$, $\mathbf{x}_j \in \mathbb{R}^d$ and $\mathbf{x} = \{x_{1j}, x_{2j}, \ldots, x_{dj}\}$, $N_i(\mathbf{x}_j)$ is the approximation function of node $i$ evaluated at $\mathbf{x}_j$. The consistency condition of the approximation function is given by [10]

$$\mathbf{p}(\mathbf{x}_j) = \sum_i N_i(\mathbf{x}_j)\mathbf{p}(\mathbf{x}_i), \tag{A.3}$$

where $\mathbf{p}(\mathbf{x}_j)$ is a vector of monomial basis functions. For a quadratic basis, $\mathbf{p} = \{1\ x\ x^2\}$ in 1D and $\mathbf{p} = \{1\ x\ y\ x^2\ y^2\ xy\}$ in 2D.

**Theorem 4.** *Given a generalized approximation in the form of Eq.* (A.1) *and a quadratic consistency condition in the form of Eq.* (A.3), *the positivity condition of the approximation function* $N_i(\mathbf{x}_j)$ (*Eq.* (8))

$$N_i(\mathbf{x}_j) >= 0 \tag{A.4}$$

*is satisfied if and only if* $N_i(\mathbf{x}_j)$ *has the Kronecker delta property*

$$N_i(\mathbf{x}_j) = \begin{cases} 1 & i = j, \\ 0 & i \neq j. \end{cases} \tag{A.5}$$

**Proof.** It is easy to see that if the approximation function $N_i(\mathbf{x}_j)$ has the Kronecker delta property, the positivity condition (Eq. (A.4)) is satisfied immediately. Conversely, if Eq. (A.4) holds, consider the following function

$$\hat{u}(\mathbf{x}) = \|\mathbf{x} - \mathbf{x}_j\|^2 = (x_1 - x_{1j})^2 + (x_2 - x_{2j})^2 + \cdots + (x_d - x_{dj})^2, \tag{A.6}$$

where $\mathbf{x} = [x_1, x_2, \ldots, x_d]^{\mathrm{T}}$ are the $d$-dimensional coordinates. The approximation of $u(\mathbf{x}_j)$ can be written as

$$u^{a}(\mathbf{x}_j) = \sum_i N_i(\mathbf{x}_j)\hat{u}(\mathbf{x}_i) = \sum_i N_i(\mathbf{x}_j)\|\mathbf{x}_i - \mathbf{x}_j\|^2. \tag{A.7}$$

Given that the approximation satisfies second-order consistency, we have

$$\sum_i N_i(\mathbf{x}_j)\|\mathbf{x}_i - \mathbf{x}_j\|^2 = \|\mathbf{x}_j - \mathbf{x}_j\|^2 = 0. \tag{A.8}$$

Given the positivity condition (Eq. (A.4)) and $\|\mathbf{x}_i - \mathbf{x}_j\|^2 > 0$ for $i \neq j$, we conclude that $N_i(\mathbf{x}_j) = 0$ for $i \neq j$, i.e.,

$$\left.\begin{array}{l} \sum_i N_i(\mathbf{x}_j)\|\mathbf{x}_i - \mathbf{x}_j\|^2 = 0 \\ N_i(\mathbf{x}_j) >= 0 \\ \|\mathbf{x}_i - \mathbf{x}_j\|^2 > 0 \text{ for all } i \neq j \end{array}\right\} \Rightarrow N_i(\mathbf{x}_j) = 0 \text{ for all } i \neq j. \tag{A.9}$$

Furthermore, the consistency conditions of the approximation require that

$$\sum_i N_i(\mathbf{x}_j) = 1. \tag{A.10}$$

Since we have $N_i(\mathbf{x}_j) = 0$ for all $i \neq j$ from Eq. (A.9), it is apparent that

$$N_i(\mathbf{x}_i) = 1. \tag{A.11}$$

Therefore, Eqs. (A.9) and (A.11) gives the Kronecker delta property for the approximation function. □

## Appendix B. Positivity of the approximation function and its derivatives in 2D

In two-dimensional kernel/least-squares approximation, the positivity conditions can be satisfied when the weighting function and the cloud points are well selected. The basic idea is to choose a well-balanced cloud. To define a balanced cloud, as shown in Fig. 24, the cloud is divided into four quadrants. Each quadrant is assumed to have the same number of points. Given the positivity conditions defined in Eqs. (8)–(10), denote the Laplacian of the approximation function of a point $\mathbf{x}_i$ and evaluated at a point $\mathbf{x}_j$ as $\nabla^2 N_i(\mathbf{x}_j)$, the weight at point $(x_i, y_i)$ as $w_i = w(x_i - x_j, y_i - y_j)$ and, for a point $\mathbf{x}_i$,

$$\begin{aligned} hx_i &= x_i - x_j, \\ hy_i &= y_i - y_j. \end{aligned} \tag{B.1}$$

It is natural to view a cloud as balanced if the center of gravity of the cloud is close to the star node (note that the weight of a point can be viewed as the mass of that point). Therefore, the criteria based on the center of gravity is given by

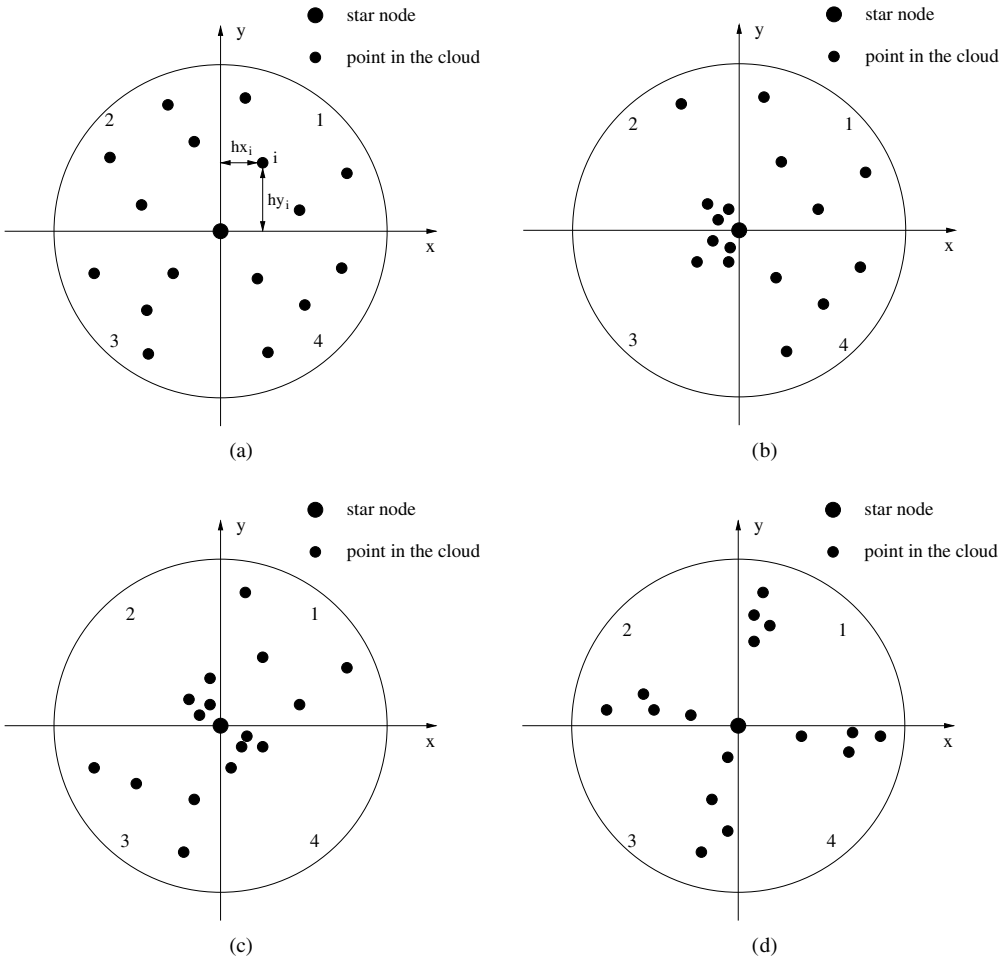


Fig. 24. (a) A balanced cloud, (b) an unbalanced cloud (type 1), (c) an unbalanced cloud (type 2), (d) an unbalanced cloud (type 3).

$$\frac{\sum_l w_l hx_l}{\sum_l w_l} \approx 0 \quad \frac{\sum_l w_l hy_l}{\sum_l w_l} \approx 0. \tag{B.2}$$

The example cloud shown in Fig. 24(b) is not a balanced cloud and this can be detected by using Eq. (B.2). Even though the clouds shown in Fig. 24(c) and (d) satisfy Eq. (B.2), i.e., the center of gravity of the cloud is close to the star node, these clouds are not defined as balanced clouds either. Thus, the center of gravity approach does not provide a sufficient criteria for determining a balanced cloud. To avoid the situations shown in Fig. 24(b)–(d), we propose a requirement for the point distribution within a cloud which is given by

$$\min\left(\sum_l w_l hx_l^2, \sum_l w_l hy_l^2\right) \gg \max\left(\sum_l w_l hx_l hy_l, \frac{\sum_l w_l hx_l \sum_l w_l hy_l}{\sum_l w_l}\right), \tag{B.3}$$

$$\min\left(\sum_l w_l hx_l^4, \sum_l w_l hx_l^2 hy_l^2, \sum_l w_l hy_l^4\right) \gg \max\left(\sum_l w_l hx_l^3 hy_l, \sum_l w_l hx_l hy_l^3\right). \tag{B.4}$$

Eqs. (B.3) and (B.4) are proposed not only to meet the criteria of the center of gravity but also to balance the mass moment of inertia for the cloud. By imposing the requirements of Eqs. (B.3) and (B.4), the analytical expressions for the approximation function and its derivatives can be simplified and it is easy to show that Eq. (B.3) avoids the situations of Fig. 24(b) and (c) and Eq. (B.4) avoids the situations of Fig. 24(d). These requirements are satisfied if the points in the cloud are spread evenly around the star point, as shown in Fig. 24(a).

With the requirements of Eqs. (B.3) and (B.4), the Laplacian of the approximation function, $\nabla^2 N_i(\mathbf{x}_j)$, can then be written as

$$\nabla^2 N_i(\mathbf{x}_j) = a_1 + a_2(x_i - x_j)^2 + a_3(y_i - y_j)^2, \tag{B.5}$$

where

$$\begin{aligned} a_1 &= \frac{2(-CD + BE + CE - BF)}{-(C^2D - 2BCE + AE^2 + B^2F - ADF)}, \\ a_2 &= \frac{2(BC - C^2 - AE + AF)}{-(C^2D - 2BCE + AE^2 + B^2F - ADF)}, \\ a_3 &= \frac{2(-B^2 + BC + AD - AE)}{-(C^2D - 2BCE + AE^2 + B^2F - ADF)} \end{aligned} \tag{B.6}$$

and

$$A = \sum_l w_l \quad B = \sum_l w_l hx_l^2 \quad C = \sum_l w_l hy_l^2 \quad D = \sum_l w_l hx_l^4 \quad E = \sum_l w_l hx_l^2 hy_l^2 \quad F = \sum_l w_l hy_l^4.$$

In Eq. (B.6), $-(C^2D - 2BCE + AE^2 + B^2F - ADF)$ is the determinant of the moment matrix (Eq. (5)). Since the moment matrix is positive definite [17], its determinant is greater than zero. For reasons discussed in Section 5, we choose the weighting function such that $w_j \gg w_i (i \neq j)$. Therefore, it is easy to show that $A \gg B, C, D, E, F$. Finally, the sign of $\nabla^2 N_i(\mathbf{x}_j)$ is determined by

$$\sum_l w_l \sum_l w_l hy_l^2 (hy_l^2 - hx_l^2) hx_i^2 + \sum_l w_l \sum_l w_l hx_l^2 (hx_l^2 - hy_l^2) hy_i^2 \tag{B.7}$$

let

$$w_l = \frac{1}{r_l^4 + \epsilon}. \tag{B.8}$$

Then the expression in Eq. (B.7) can be rewritten as

$$\sum_l \frac{\cos^2(2\theta_l) - \cos(2\theta_l)}{2} hx_i^2 + \sum_l \frac{\cos^2(2\theta_l) + \cos(2\theta_l)}{2} hy_i^2, \tag{B.9}$$

where

$$\cos(\theta_l) = \frac{hx_l}{r_l}. \tag{B.10}$$

It is clear that if $\sum_l \frac{\cos^2(2\theta_l)-\cos(2\theta_l)}{2}$ and $\sum_l \frac{\cos^2(2\theta_l)+\cos(2\theta_l)}{2}$ are greater than zero, $\nabla^2 N_i(\mathbf{x}_j)$ is positive for any $hx_i$ and $hy_i$. Define

$$f_1(\theta_l) = \cos^2(2\theta_l) - \cos(2\theta_l), \tag{B.11}$$

$$f_2(\theta_l) = \cos^2(2\theta_l) + \cos(2\theta_l). \tag{B.12}$$

Look at the quadrant where $0 \leqslant \theta_l \leqslant \frac{\pi}{2}$. Given a $\theta_1$ within $[0, \frac{\pi}{4}]$ and a $\theta_2$ within $[\frac{\pi}{4}, \frac{\pi}{2}]$, we have

$$f_1(\theta_1) < 0 \quad \text{and} \quad f_1(\theta_2) > 0, \tag{B.13}$$

$$\min(f_1(\theta_1)) = -\frac{1}{4}. \tag{B.14}$$

If we choose $\theta_2$ such that $f_1(\theta_2) \geqslant \frac{1}{4}$, then $f_1(\theta_1) + f_1(\theta_2) \geqslant 0$. In this case, we obtain

$$\frac{\arccos\left(\frac{1-\sqrt{2}}{2}\right)}{2} \leqslant \theta_2 \leqslant \frac{\pi}{2}. \tag{B.15}$$

Similarly,

$$f_2(\theta_1) + f_2(\theta_2) \geqslant 0 \;\rightarrow\; 0 \leqslant \theta_1 \leqslant \frac{\arccos\left(\frac{\sqrt{2}-1}{2}\right)}{2}. \tag{B.16}$$

Since $\frac{\arccos(\frac{1-\sqrt{2}}{2})}{2} \approx 51°$ and $\frac{\arccos(\frac{\sqrt{2}-1}{2})}{2} \approx 39°$, we can conclude that, if Eqs. (B.3) and (B.4) is satisfied for a given cloud, one can construct the fixed kernel approximation and satisfy the positivity conditions by employing a weighting function of Eq. (B.8) and selecting the same number of points in $[\frac{n\pi}{2}, 39° + \frac{n\pi}{2}]$ and $[51° + \frac{n\pi}{2}, 90° + \frac{n\pi}{2}], n = 0, 1, 2, 3$.

## References


[1] T. Belytschko, Y. Krongauz, D. Organ, M. Fleming, P. Krysl, Meshless methods: an overview and recent developments, Comput. Methods Appl. Mech. Engrg. 139 (1996) 3–47.

[2] X. Jin, G. Li, N.R. Aluru, On the equivalence between least-squares and kernel approximation in meshless methods, CMES: Comput. Model. Engrg. Sci. 2 (4) (2001) 447–462.

[3] T. Belytschko, Y.Y. Lu, L. Gu, Element free Galerkin methods, Int. J. Numer. Methods Engrg. 37 (1994) 229–256.

[4] W.K. Liu, S. Jun, S. Li, J. Adee, T. Belytschko, Reproducing kernel particle methods for structural dynamics, Int. J. Numer. Methods Engrg. 38 (1995) 1655–1679.

[5] J.-S. Chen, C. Pan, C. Wu, W.K. Liu, Reproducing kernel particle methods for large deformation analysis of non-linear structures, Comput. Methods Appl. Mech. Engrg. 139 (1996) 195–227.
[6] S.N. Atluri, T. Zhu, A new meshless local Petrov–Galerkin (MLPG) approach in computational mechanics, Comput. Mech. 22 (1998) 117–127.
[7] E. Oñate, S. Idelsohn, O.C. Zienkiewicz, R.L. Taylor, A finite point method in computational mechanics. Applications to convective transport and fluid flow, Int. J. Numer. Methods Engrg. 39 (1996) 3839–3866.
[8] E. Oñate, S. Idelsohn, O.C. Zienkiewicz, R.L. Taylor, C. Sacco, A stabilized finite point method for analysis of fluid mechanics problems, Comput. Methods Appl. Mech. Engrg. 139 (1996) 315–346.
[9] T.J. Liszka, C.A. Duarte, W.W. Tworzydlo, hp-Meshless cloud method, Comput. Methods Appl. Mech. Engrg. 139 (1996) 263–288.
[10] N.R. Aluru, A point collocation method based on reproducing kernel approximations, Int. J. Numer. Methods Engrg. 47 (2000) 1083–1121.
[11] N.R. Aluru, G. Li, Finite cloud method: a true meshless technique based on a fixed reproducing kernel approximation, Int. J. Numer. Methods Engrg. 50 (10) (2001) 2373–2410.
[12] J.J. Benito, F. Urena, L. Gavete, Influence of several factors in the generalized finite difference method, Appl. Math. Model. 25 (2001) 1039–1053.
[13] T.S. Motzkin, W. Wasow, On the approximation of linear elliptic differential equations by difference equations with positive coefficients, J. Math. Phys. 31 (1953) 253–259.
[14] S.V. Patankar, Numerical Heat Transfer and Fluid Flow, Hemisphere, 1980.
[15] L. Demkowicz, A. Karafiat, T. Liszka, On some convergence results for FDM with irregular mesh, Comput. Methods Appl. Mech. Engrg. 42 (1984) 343–355.
[16] I.N. Bronshtein, K.A. Semendyayev, Handbook of Mathematics, Springer-Verlag, Berlin, Heidelberg, 1998.
[17] W. Han, X. Meng, Error analysis of the reproducing kernel particle method, Comput. Methods Appl. Mech. Engrg. 190 (2001) 6157–6181.
[18] P. Krysl, T. Belytschko, Element-free Galerkin method: convergence of the continuous and discontinuous shape functions, Comput. Methods Appl. Mech. Engrg. 148 (1997) 257–277.
[19] W.K. Liu, S. Li, T. Belytschko, Moving least-square reproducing kernel methods (I) methodology and convergence, Comput. Methods Appl. Mech. Engrg. 143 (1997) 113–154.
[20] S.C. Brenner, L.R. Scott, The Mathematical Theory of Finite Element Methods, Springer, New York, 1994.
[21] I. Babuska, J.M. Melenk, The partition of unity method, Int. J. Numer. Methods Engrg. 40 (1997) 727–758.
[22] G.H. Golub, C.F. Van Loan, Matrix Computations, Johns Hopkins University Press, 1989.
[23] Y. Krongauz, T. Belytschko, Enforcement of essential boundary conditions in meshless approximations using finite elements, Comput. Methods Appl. Mech. Engrg. 131 (1996) 133–145.
[24] A. Huerta, S. Fernandez-Mendez, Enrichment and coupling of the finite element and meshless methods, Int. J. Numer. Methods Engrg. 48 (2000) 1615–1636.
[25] G.J. Wagner, W.K. Liu, Hierarchical enrichment for bridging scales and meshfree boundary conditions, Int. J. Numer. Methods Engrg. 50 (2001) 507–524.
[26] J.S. Chen, W. Han, Y. You, X. Meng, A reproducing kernel method with nodal interpolation property, Int. J. Numer. Methods Engrg. 56 (2003) 935–960.
[27] S.P. Timoshenko, J.N. Goodier, Theory of Elasticity, McGraw-Hill, 1982.